buildings

Article

The Rehabilitation of the Historical Bridge of Konitsa, Epirus, Greece: A Documentation-Based Methodology of Structural Analysis and Rehabilitation Strategy

Christos Giannelos, Vasiliki Palieraki, Erato Oikonomopoulou and Elizabeth Vintzileou *

Department of Structural Engineering, School of Civil Engineering, National Technical University of Athens, 15773 Athens, Greece; cgian@mail.ntua.gr (C.G.); vasopal@central.ntua.gr (V.P.); eratooikonomopoulou@central.ntua.gr (E.O.)
* Correspondence: elvintz@central.ntua.gr; Tel.: +30-210-772-1272

Abstract: The bridge of Konitsa over the Aoos river, in Epirus, Greece, was built in 1869. It is one of the most important stone arched bridges in the Balkans, listed by the Hellenic Ministry of Culture (1982). The bridge, damaged by the Ottoman Army in 1913, was restored the same year by French engineers using reinforced concrete. Structural deterioration, located mainly in the area damaged by the explosion and subsequently repaired, led to the study of the bridge by the National Technical University of Athens (NTUA), in the framework of a Contract among the Prefecture of Epirus, the Municipality of Konitsa (owner of the bridge), the Ministry of Culture and NTUA. The entire study includes the exhaustive documentation of the bridge, its numerical modelling and assessment at its current state, the selection of adequate interventions and the numerical investigation of the efficiency of the proposed interventions. During this process, one of the main issues was the treatment of the concrete intervention of 1913. For the choice and for the design of the restoration measures, a calculation methodology was adopted, based on the findings of the documentation of the bridge, while taking into account the critical phases (construction, damage and repair) over its lifetime. This work has proven the available safety of the bridge under its self-weight, as well as the need for reconstruction of the RC jacket at the intrados of the arch, which was applied as a repair measure to the bridge in 1913.

Keywords: arched stone bridge; documentation; assessment; rehabilitation

check for updates

Citation: Giannelos, C.; Palieraki, V.; Oikonomopoulou, E.; Vintzileou, E. The Rehabilitation of the Historical Bridge of Konitsa, Epirus, Greece: A Documentation-Based Methodology of Structural Analysis and Rehabilitation Strategy. *Buildings* **2024**, *14*, 690. https://doi.org/10.3390/buildings14030690

Academic Editor: Rajai Zuheir Al-Rousan

Received: 29 January 2024
Revised: 14 February 2024
Accepted: 27 February 2024
Published: 5 March 2024

1. Introduction

The documentation (in situ and in-laboratory) of arch stone bridges, the investigation of their behaviour under vertical loads, in seismic conditions, as well as the effect of soil conditions, constitute a topic of interest for numerous researchers due to the large number of heritage bridges in need of assessment, repair and upgrading. The investigation of the behaviour of the case study bridges includes modelling and numerical calculations, based on several commercial or research-oriented pieces of software. Several methods of analysis, simplified or sophisticated, were applied, namely, linear elastic, nonlinear static, linear and nonlinear dynamic, using 2- or 3D models, etc. The exhaustive evaluation of the relevant publications is beyond the scope of this work. Nonetheless, more than thirty (30) publications were studied with the purpose of (a) identifying works including the full documentation of one or more bridges, and numerical calculations either to assess the current margin of safety or to investigate the efficiency of the intervention schemes, and (b) evaluating the results of the numerical analyses performed using various methods, in order for the authors of this paper to make decisions on the method of analysis to be applied within the current work, taking into account its objective.

Extensive investigations for the documentation of the examined bridges are reported in [1], (on-site tests on masonry, observation through endoscopy, a survey of pathology, etc.), in [2] (geometrical survey, geotechnical investigations, a survey of pathology, sampling and testing of materials, etc.), in [3] (building of a geometrically accurate model of the studied bridge, including its pathology, use of georadar scans to identify the dimensions of various structural components, etc.), and in [4] (geometrical survey, geotechnical investigation, sonic tests in combination with endoscopy to identify the construction typology of piers, etc.). In other studies, focusing on the modelling and the numerical calculations, although specific historical arch bridges are used as case studies, the data that needed to be implemented in the numerical models are mostly assumed, based on the literature or values of properties proposed by Codes or Guidelines are adopted (e.g., [5–10]).

Several works deal with the dynamic identification of historical bridges, with the purpose of assessing their seismic behaviour, through comparison of in situ dynamic tests and results of numerical calculations (e.g., [2,11,12]), whereas in [13], the authors used the results of in situ dynamic identification tests for comparison with the numerical calculations, with the purpose of assessing the effect of temperature changes on the natural frequencies of a historical bridge.

In other studies, the purpose was to evaluate the capacity of historical (roadway or railway) arch bridges under vertical traffic loads (either centric or eccentric). In the respective calculations, load tests of the bridges were performed (e.g., [4,10,14]).

There are studies in which scaled arches were subjected to laboratory tests, while their behaviour was predicted through numerical calculations (e.g., [15], where the specific case of the behaviour of arches against high-rate loads is investigated).

In all the studies, whether they include full documentation of bridges or not, there is an element of modelling and numerical calculations, while there are studies that are purely analytical, although the geometry of an existing bridge is modelled (e.g., [9,16,17]).

Regarding the modelling and the numerical calculations, the entire range of available methods (an overview is included in [18] and in [19] for nonlinear seismic methods) is used in various studies. Thus, mostly on FE models of arch bridges, linear elastic, nonlinear static (pushover) and dynamic analyses, response spectrum, rigid block limit analysis, as well as time history elastic or inelastic analyses are performed. In some cases, operational model analyses are performed, including model updating (e.g., [11,13]). As for the models and failure criteria adopted for masonry, in nonlinear analyses, various assumptions are made, namely, elastic–plastic (e.g., [5]), total strain crack model (e.g., [20]), Drucker–Prager failure criterion, the deterioration model [21], etc., depending on the purpose of the analytical work. It is noted that in several cases, although an existing bridge is considered, with surveyed pathology, no explicit comparison with the observed damage is provided in the publications. In many cases though, such a comparison with the pathology is provided, allowing for the efficiency of the numerical calculations to be assessed (e.g., [1,15,22–24]).

Several researchers (e.g., [8,19]) comment on the difficulties in defining the parameters related to the elastic and inelastic behaviour of masonry (such as E-modulus, Poisson's ratio, fracture parameters, etc.) when implemented in software applicable to nonlinear analyses, even after the masonry bridge and its constituent materials are documented. They also comment on the sensitivity of the obtained numerical results on the assumed masonry properties.

Finally, researchers that have applied both elastic and inelastic methods of analysis (e.g., [1,2,6,12]) report on the efficiency of all the applied methods to identify the critical regions, as well as the modal shapes of the bridge.

This brief and definitely incomplete survey of the literature, proving the significance of the topic and the need to preserve old masonry arch bridges, is enlightening in terms of the importance of the documentation, of the difficulties encountered when several properties of masonry are to be estimated, even based on exhaustive documentation, and the need to choose an adequate methodology for numerical calculations, in accordance with the available data and the scope of each specific study.

This study presents the methodology followed for the numerical modelling and the parametric analyses performed to assist decision-making related to the rehabilitation of the historical arch bridge of Konitsa. The value of this methodology is that it is based on the exhaustive documentation of the bridge studied by Palieraki et al. [25]. This documentation has not only provided reliable data on the properties of materials and the construction typology of masonry in various regions of the bridge, but it has also dictated a step-by-step calculation of the action–effects (forces and deformations), following the construction phases of the bridge, as well as its behaviour before and after the damage induced by the attempt to destroy the bridge using explosives in 1913. Following this man-induced damage, in the region of the crown of the arch, plain concrete was used to fill the damaged region. In addition to this, a reinforced concrete jacket was constructed at the intrados of the bridge, the time of this intervention being unidentified when this study was initiated. Actually, the need for this study arose from the poor condition of the reinforced concrete jacket at the intrados of the arch, which exhibits pronounced disintegration of the concrete as it falls into pieces, as well as extensive and severe corrosion of the reinforcement. As the bridge is a monument, listed by the Hellenic Ministry of Culture (since 1982), the preference of the Authorities was to remove the RC jacket. However, such a decision should be based on the identification of the time that intervention was applied, as well as on the interpretation of its structural function.

To obtain reliable data and to propose a credible and efficient scheme of interventions for the preservation of the bridge, exhaustive documentation of the bridge was planned and executed. As presented in [25], the documentation included an investigation of the geotechnical conditions at the south bank of the river (the north abutment being founded on rock), the identification of the bridge's structural system, the elaborate survey of its pathology, the application of in situ non-destructive investigation techniques to identify the typology of the masonry construction and the extensive sampling and laboratory testing of materials that were carefully selected from various regions of the monument. It is noted that the study of historical data related to the bridge did not allow for the time of construction of the RC jacket at the intrados to be identified.

The obtained results made possible the development of a geometrically and mechanically accurate numerical model of the bridge. Furthermore, the hydraulic study of the region has provided the data that are necessary for the assessment of the risk against flood. Finally, the seismic actions for the region, as prescribed by the relevant Code in force, were considered to estimate the margin of safety of the bridge against earthquakes.

The methodology adopted for the numerical calculations and their rationale is presented herein, along with selected results of those calculations, confirming the observed pathology and assisting the decision-making related to the interventions that are necessary for the preservation of the historical bridge.

2. Brief Description of the Bridge and Review of Documentation

Both a detailed description of the historical bridge and the results of the documentation campaign are presented in [25]. Nonetheless, for the benefit of the readers of this paper, some basic data and findings are repeated herein.

The bridge of Konitsa is an arch stone bridge, constructed in 1869. It consists of a central arch (36.90 m in diameter) and two abutments (Figure 1). The total length of the bridge at the level of the parapets is equal to 60.50 m. Its width at the level of the pavement varies between 2.90 m at the crown of the arch and 3.30 m at the end of the abutments. The arch consists of two superimposed arches, the main arch (at the intrados) and the secondary one (at the extrados), as shown in Figure 2a. The main arch is in recess (by 5.50 cm to 6.50 cm) with respect to the secondary one, whereas the construction of the abutments follows the width of the secondary arch.

The main arch is 75 cm~80 cm high and it is provided with eighteen (18) transverse metal connectors (Figure 2b). The height of the secondary arch is equal to 60 cm approximately in the region between its springing level and an angle of about 45°, whereas it is reduced to approximately 50 cm at the central area of the arch. Both the main and the secondary arches are made of schist stones. The thickness of the stones varies between 6 cm and 10 cm and the mortar joints are thin, with an average thickness of 10 mm.

Figure 1. Konitsa historical bridge—upstream view.

(**a**) (**b**)

Figure 2. Construction details: (**a**) portion of the arch (between 45° and 60° from its theoretical support), view of the N-abutment from downstream; (**b**) detail of the anchorage of transverse metal connector.

The documentation plan [25] included the following: (a) the collection and evaluation of historical data, including its "structural history"; (b) a geometrical survey, using conventional and photogrammetric techniques (Figure 3, [26]); (c) a survey of morphological characteristics and identification of the bearing system of the bridge, using georadar scans and observation through borescopy; (d) the sampling of materials and laboratory tests to identify their chemical and mechanical properties; (e) a geotechnical investigation; and (f) the investigation of the hydraulic and seismic conditions of the region affecting the bridge.

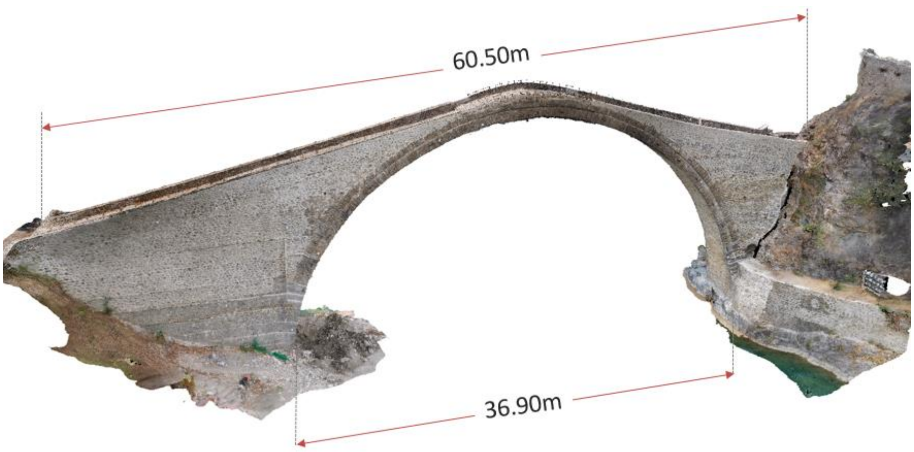

Figure 3. Photogrammetric 3D model by Michaelidis [26], upstream view.

According to the historical data, the construction of the bridge in 1869 was funded mainly by the entrepreneur I. Loulis, who funded the construction (three years earlier) of the historical bridge of Plaka. There is a mention in the sources [27] that the sponsor requested the same technicians to also work for the construction of the Konitsa bridge. This historical evidence, along with the morphological and constructional similarities of the two bridges (Figure 4), has suggested that the already studied Plaka bridge [28] could serve as a case adequate for comparison with the Konitsa bridge. Indeed, both bridges were built following similar construction phases, while—guided by the documentation of the Plaka bridge—the authors were able to identify similar construction details in the Konitsa bridge. As an example of the similarities between the two bridges, it was mentioned that in the main arch of the bridge of Konitsa, both at its intrados and on its (upstream and downstream) faces, holes are visible (Figure 5a). An investigation using georadar and borescope revealed [25] the locations of timber grids (at an advanced stage of disintegration), which consist of two components, namely, inclined grids connecting the two arches and following their curvature (Figure 5b) and horizontal grids in the abutments (Figure 5c). The horizontal and inclined timber grids were connected using iron nails. Such timber grids were found in the bridge of Plaka as well [28]. The structural role of the horizontal timber grids, identified and numerically confirmed in [25,28], is explained herein as well.

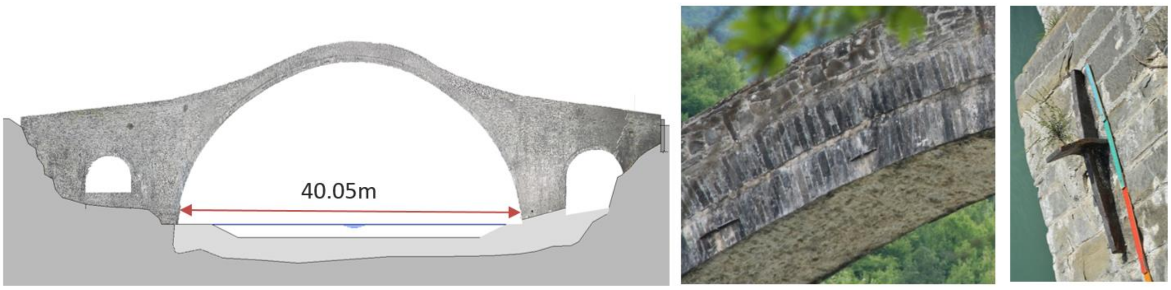

(**a**)

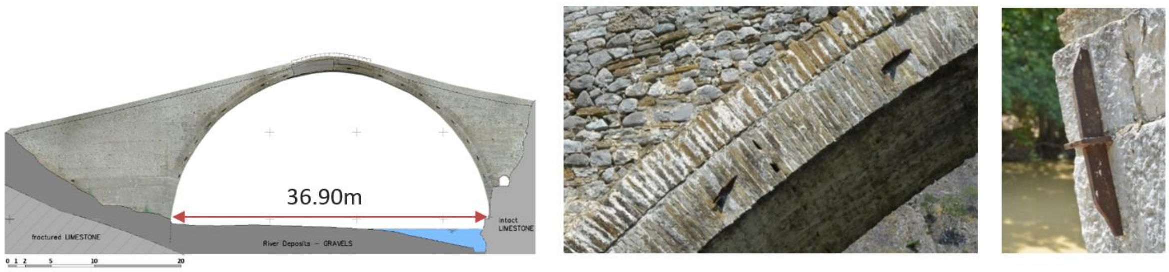

(**b**)

Figure 4. Comparison between Plaka bridge and Konitsa bridge (details of arch construction and of anchorage of iron connectors): (**a**) Plaka bridge—downstream view; (**b**) Konitsa bridge—upstream view.

The Konitsa bridge, as well as that of Plaka, was constructed in two phases, namely, the abutments (including the springing of the arch) were constructed first, with formwork needed only for the portion of the arch. Subsequently, i.e., a few months later, the central part of the arch was constructed, after the installation of the necessary scaffold and formwork. This procedure, documented for the bridge of Konitsa in [25] and for the bridge of Plaka in [28], dictated the methodology of numerical calculations, as presented in Section 5.

As aforementioned, there was an attempt to destroy the bridge by the retreating Ottoman army in 1913. Despite a significant loss of mass in the critical region of the arch (close to its crown, Figure 6a [29]), the bridge did not collapse. The engineers of the French Army that repaired the bridge the same year (Figure 6b) filled the holes due to the explosion with plain concrete (Figure 7a). This concrete is in good condition. Its compressive strength, based on the rebound technique, was estimated to be 50 MPa. The measured carbonation depth is limited [25]. In the same damaged region, at the intrados of the arch, there is an RC jacket (Figure 7b), in very poor condition. Laboratory tests on samples of the reinforcement of this jacket have proven that this intervention was part of the 1913 repair of the bridge [25]. Thus, the question arose about the structural function of this jacket. The answer to this question would guide decision-making on whether the RC jacket was to be removed or reconstructed using durable materials.

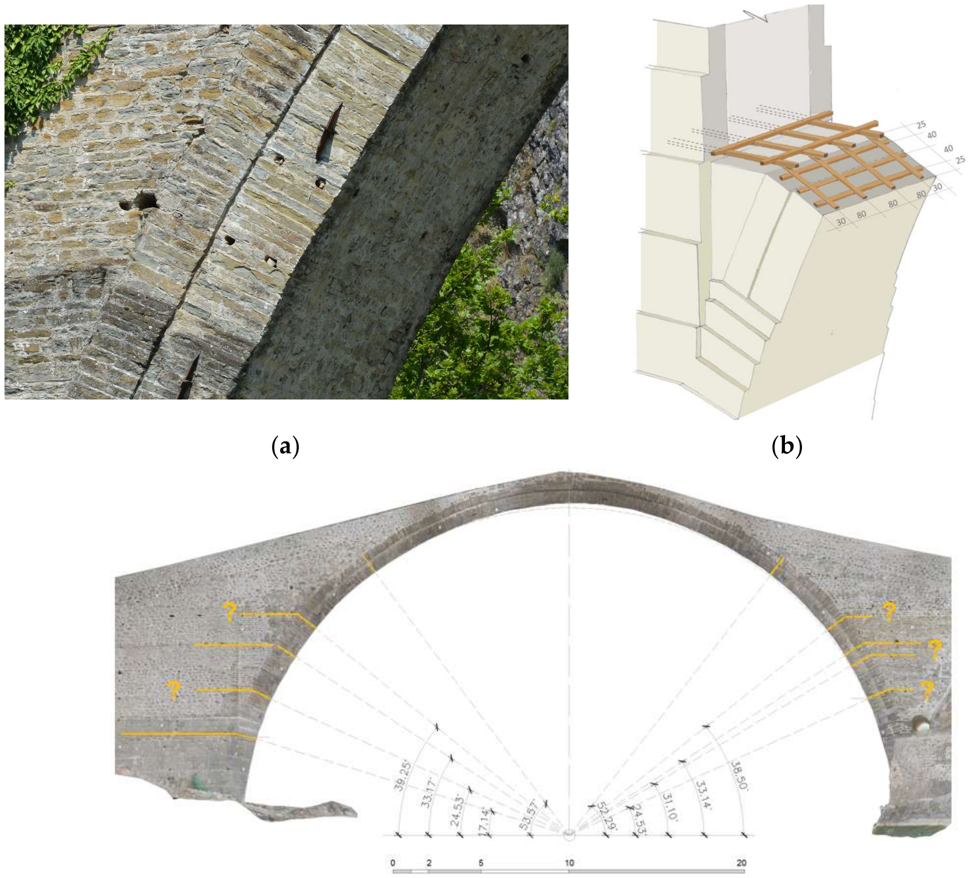

(**a**) (**b**)

(**c**)

Figure 5. (**a**) View of the intrados of the arch at the location of a timber grid; the holes corresponding to the location of disintegrated timber elements are visible, (**b**) sketch showing the two timber grids (horizontal and radial) in the arch area (dimensions in cm), (**c**) graphical representation of the timber grids in the two abutments of the bridges (in yellow), as identified by georadar scanning. The end of some timber was not possible to detect (indicated with "?").

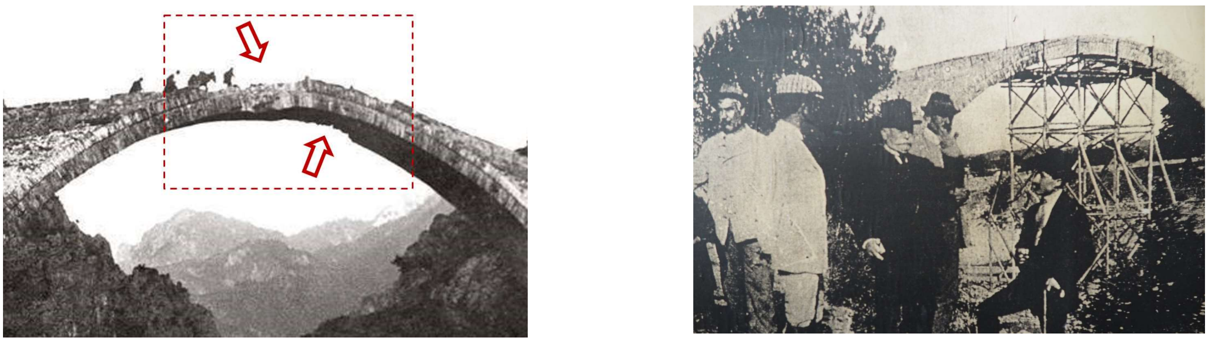

(**a**) (**b**)

Figure 6. (**a**) The damage to the central part of the arch (photo by Rhomaides-Zeitz 1913 [29]), (**b**) photo (by unknown photographer) taken during the repair of the bridge by the French Army (courtesy V. Kaskanis).

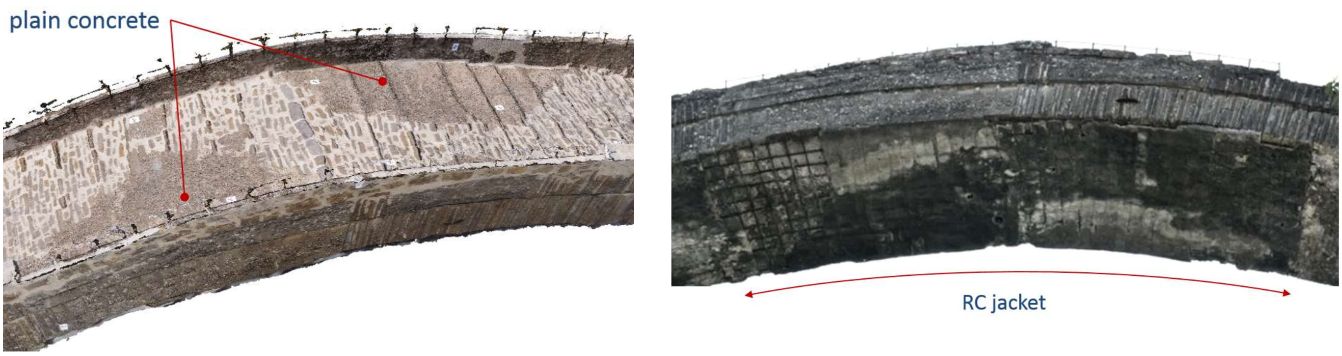

(**a**) (**b**)

Figure 7. The repair of the bridge, comprising (**a**) plain concrete filling the holes at the extrados of the arch, and (**b**) reinforced concrete jacket at the intrados of the arch.

3. Bridge Pathology

The state of the bridge is, in general, good, except for the region of the 1913 repair and, more specifically, of the RC jacket at the intrados of the arch. Nonetheless, there is damage in several locations, described herein. It is noted that the surveyed cracks and dislocations are not recent. The bridge was not subject to any intervention after 1913, with the exception of the uprooting of plants that grew in some locations and the re-pointing of masonry.

- Oblique cracks in the lower region of the south abutment Inclined cracks are observed passing through mortar joints and through stones. More specifically, cracks through the mortar joints are witnessed by the white-coloured mortar used for re-pointing, applied in 2017, Figure 8. The cracks in the stones are numbered (two of them are shown in close-up photos in the same Figure 8), while their widths range between 0.2 mm and 1.2 mm. The inclined cracks are directed from the upstream springing of the arch to the downstream base of the south abutment.
- Cracks in the arch stones at the region of its springing Almost vertical cracks are observed in the end stones of the main arch, at its intrados, in two locations, namely, in the downstream region of the south abutment, underneath the first transverse iron tie (Figure 9a), as well as at the base of the abutment (Figure 9b). Cracks of the same morphology are detected in the end stones of the arch, at the north abutment, in the region underneath the first iron connector (Figure 9c,d). In some cases, as shown in Figure 9c, there are stones detached from the arch.
- Vertical cracks in the spandrel walls Vertical cracks were surveyed by the authors in the upstream spandrel of the south abutment (Figure 10a), as well as in the downstream spandrel of the north abutment (Figure 10b) in the framework of a preliminary inspection, before the initiation of the detailed documentation.
- Missing stones at the foundation of the north abutment Although the north abutment is founded on rock, leveling works were needed to create a horizontal plane for the construction of the bridge. This was achieved through local filling using small-sized stones (Figure 11). Due to the hydraulic conditions in the area, some of the stones were detached and are missing.
- The state of the 1913 repaired region The major structural problem of the bridge is the poor condition of the RC jacket constructed at the intrados of the main arch, in the region of its crown (Figure 12), as part of the after-explosion repair of the bridge in 1913 [25]. The jacket, 100 mm to 120 mm thick, is provided with longitudinal reinforcement, consisting of eleven bars, 24 mm in diameter. Transverse bars, 14 mm in diameter were arranged, and spaced at approximately 150 mm. The grid of longitudinal and transverse bars is anchored to the arch, at its intrados, using steel hangers either wedged between stones of the arch or anchored to the plain concrete of the extrados. Smooth bars with handmade protrusions for an improved bond with the concrete were used. The RC jacket presents very advanced corrosion of the reinforcement, with

a significant reduction in the bars' diameter and disintegration of the concrete, as shown in Figure 13. Therefore, the structural function of the RC jacket is no longer fulfilled. To make a decision on whether reconstruction of the disintegrated RC jacket is needed, it is necessary to identify the reason for which that intervention was applied, and if its rationale is justified.

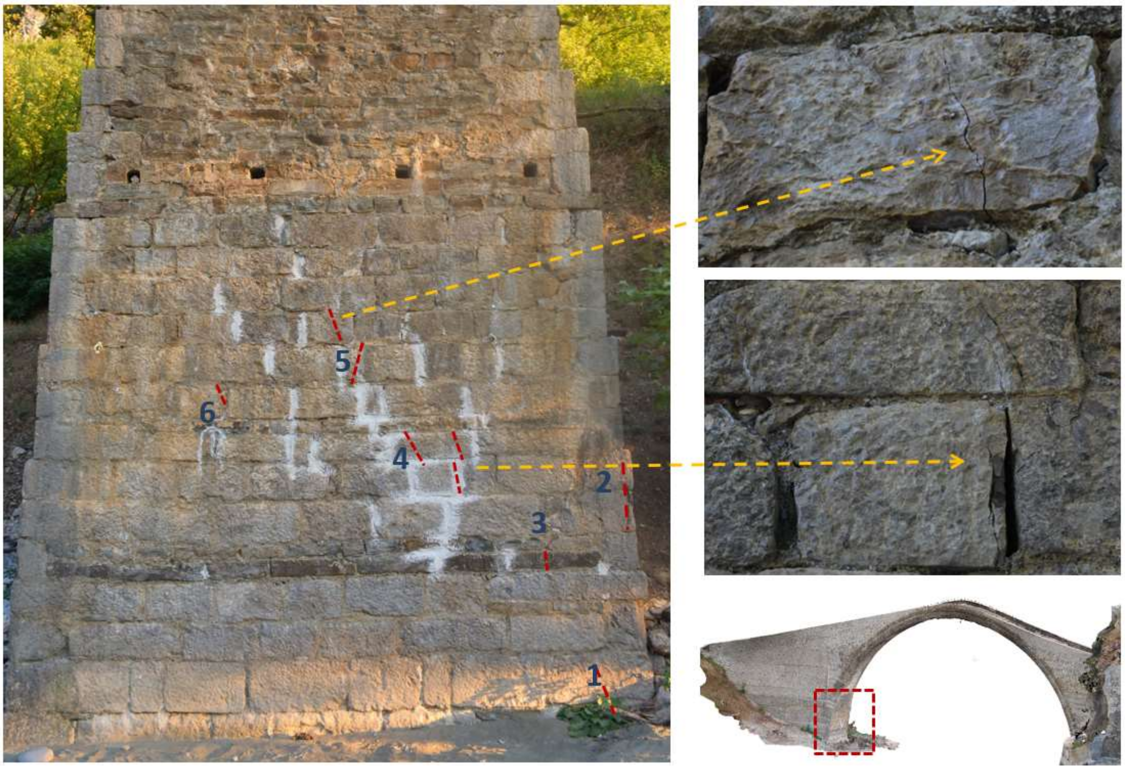

Figure 8. The inclined cracks (numbered 1 to 6) in the lower part of the south abutment of the bridge (region in the red square).

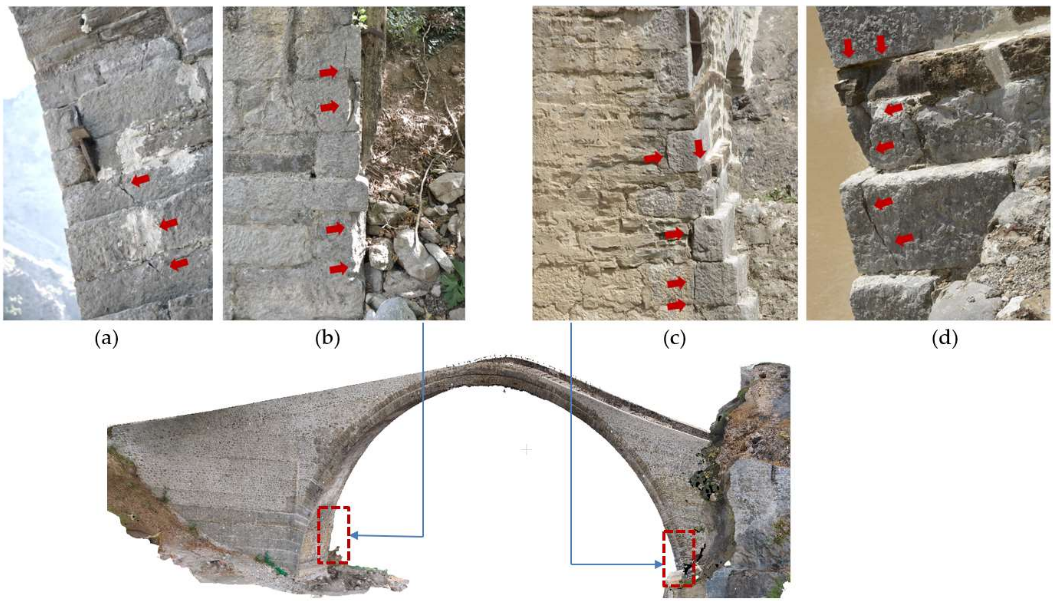

Figure 9. Damage (highlighted by red arrows) to the end stones of the main arch, at its lower part: (**a**) downstream of S-abutment, cracked stones at the region of the spring of the main arch; (**b**) cracked stones in the same region, at the base of the S-abutment; (**c**) upstream of N-abutment, cracked and detached stones at the spring of the arch, south view; (**d**) the same as in (**c**), view from upstream.

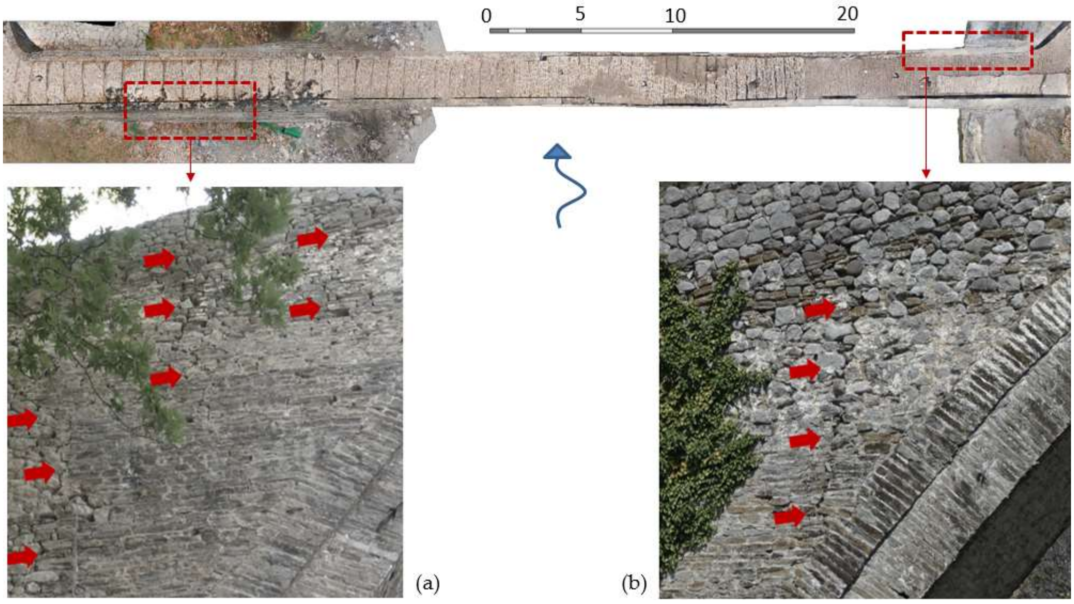

Figure 10. Vertical cracks in the spandrel walls highlighted by red arrows: (**a**) upstream spandrel wall of the south abutment; (**b**) downstream spandrel of the north abutment.

Figure 11. Stones are missing at the level of the north abutment foundation.

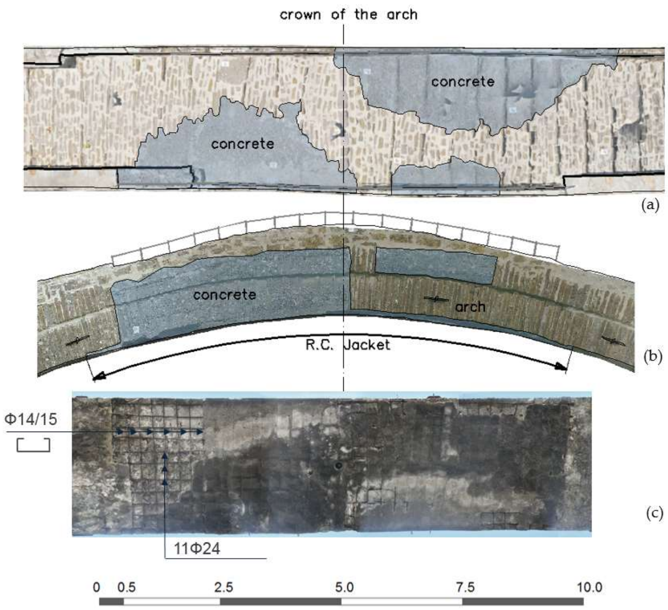

Figure 12. Geometrical survey of the after-explosion repair intervention: (**a**) plan; (**b**) upstream view; (**c**) view of the intrados of the arch. Scale in meters.

Figure 13. Condition of the RC jacket at the intrados of the arch.

4. Building the Numerical Model of the Bridge

The bridge was modelled with the software SOFISTIK (ver. 14.14–30) [30], using volume elements (Figure 14a) for masonry, shell elements for the RC jacket at the intrados of the arch (Figure 14b) and linear elements for the timber. The detailed geometry of the bridge was reproduced (Figure 15) based on its photogrammetric survey [26]. The parameters adopted for various parts of the bridge, as well as for the foundation, are presented herein. Vertical loads, mainly, the self-weight of the bridge, were considered, while, based on a hydraulic study, the accidental action of flood was accounted for. Finally, the behaviour of the bridge under seismic actions was also investigated.

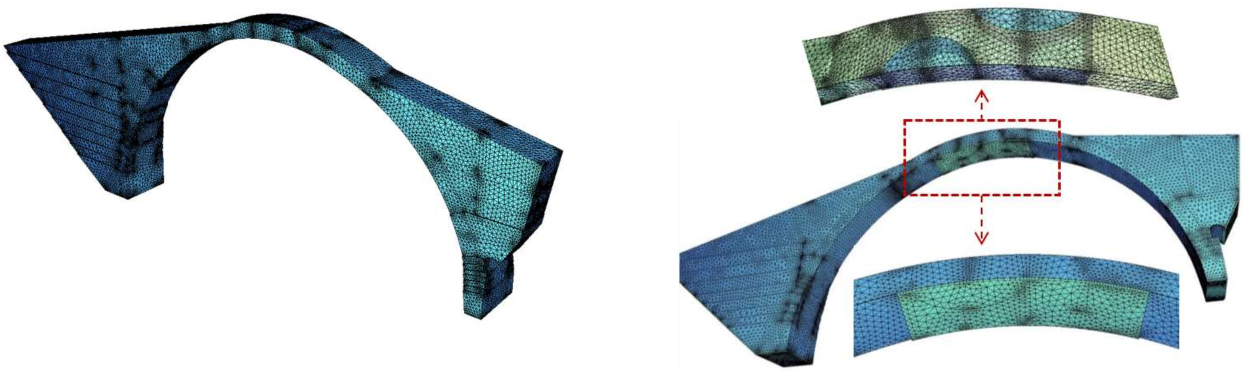

(**a**) (**b**)

Figure 14. Numerical model of the bridge: (**a**) general view of the 3D mesh; (**b**) detail of 1913 concrete intervention.

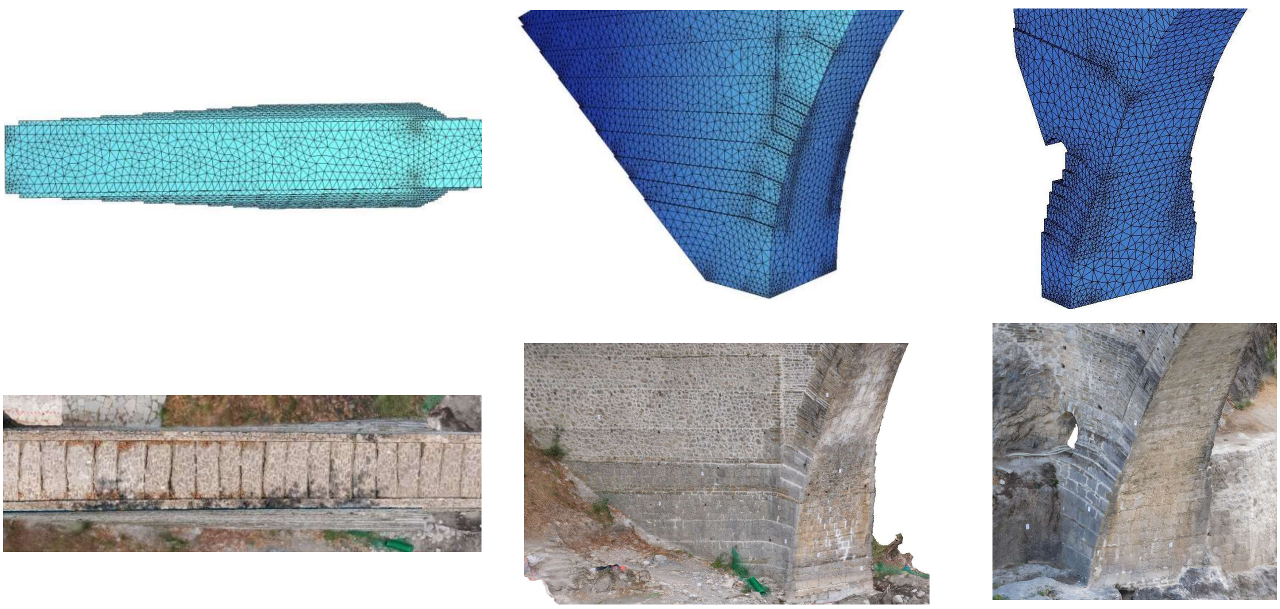

Figure 15. Accurate geometrical reproduction of the bridge in the numerical model.

4.1. Mechanical Properties of the Masonry

As shown in Figure 16a, the construction typology of the masonry is different in various regions of the bridge. Those regions, identified during the documentation of the bridge, were distinguished in the numerical model, whereas adequate material properties were adopted for each of them. As shown in Figure 16b, four regions are distinguished, namely, the arch (region "1"), the lower portion of the abutments characterised by a solid construction typology (region "2"), the spandrel walls (region "3") and the filling material between the spandrel walls (region "4"). It is noted that although there is a distinction in the mechanical properties of regions 3 and 4, a perfect bond between the exterior walls and the filling material is assumed. This is because no sign of any detachment between the spandrel walls and the filling was detected, neither during the meticulous visual inspection nor during examination using the borescope.

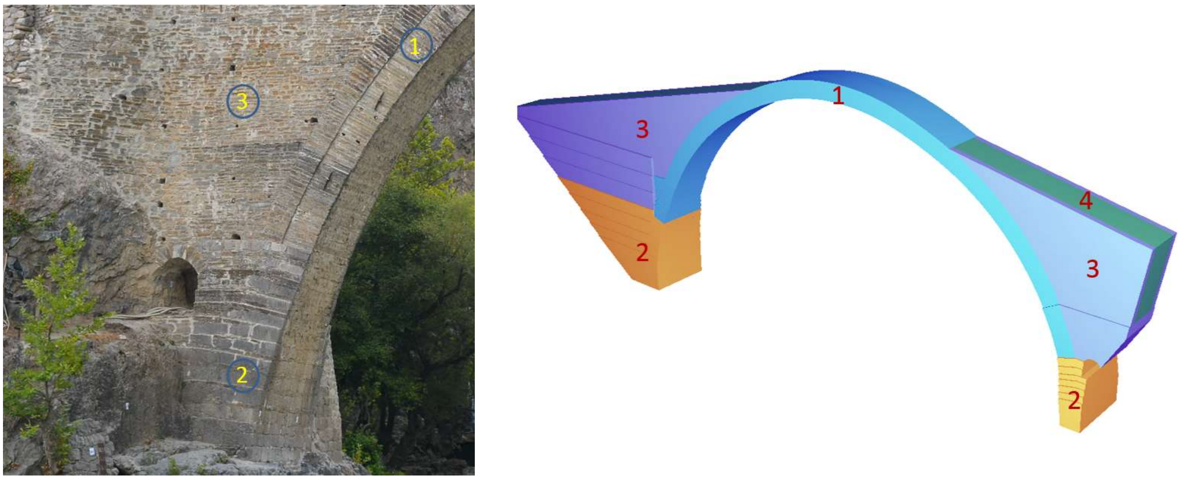

(**a**) (**b**)

Figure 16. (**a**) Construction typology of masonry in various regions of the bridge; (**b**) 3D numerical model of the bridge—identified regions of masonry characterised by different geometrical and mechanical properties (view from upstream).

The lower portion of the abutments and the arch are made with cut stones and thin mortar joints, whereas the part of the abutments between the solid base and the deck is made following the three-leaf construction typology. The spandrel walls are made with rubble or semi-cut stones and a significant volume of mortar, whereas the infill between the walls is of a rather loose and poor-quality material (a mix of stones and low-quality mortar in high percentage). As a rule, the regions closer to the arch are better constructed, using semi-cut stones. In order to estimate as reliably as possible the mechanical properties of the masonry, more specifically, its compressive strength and modulus of elasticity (Table 1), the construction typology of the masonry at each location was considered, along with the data obtained from in-lab testing of the samples taken in situ.

Table 1. Mechanical properties of masonry and concrete considered in numerical calculations.

Region Number	Area	Modulus of Elasticity (MPa)	Mean Compressive Strength f_{wc} (MPa)
1	Arch	5350 ÷ 8900	8.90
2	Abutments	8700 ÷ 14,500	14.50
3	Spandrel walls	1500 ÷ 2500	2.50
4	Filling material	500 ÷ 800	0.80
5	Concrete	27,400	20

The properties assumed for the concrete need to be commented on. As aforementioned, the application of the rebound technique to the plain concrete at the extrados of the arch has yielded values of compressive strength at around 50 MPa. Nonetheless, this concrete is carbonated (the carbonation depth varies between 20 mm and 30 mm); therefore, the measurements using the rebound technique are expected to overestimate the compressive strength of the material. Thus, a conservative value of compressive strength was assumed for the concrete (=20 MPa).

Two equations are applied to estimate the compressive strength of the masonry: for the arch and for the base of the abutments, where cut stones are used and the thickness of the mortar joints is limited, the equation included in Chapter 3.6.1.2 of Eurocode 6 [31] is applied. Nonetheless, in the equation, the mean compressive strength of the stones and the mortar are introduced, while partial safety factors equal to unity were assumed, as the purpose of the numerical work is to assess the available margins of safety of the bridge and not to design its various parts. Finally, constant K was taken equal to 0.45.

For the spandrel walls, made of rubble stone masonry, the empirical equation by Tassios and Chronopoulos [32] was applied:

$$f_{wc} = \frac{\left(\frac{2}{3} \cdot \sqrt{f_b} + k_1 \cdot f_m - k_2\right)}{\left[1 + 3.50 \cdot \left(\frac{V_m}{V_w} - 0.30\right)\right]} \tag{1}$$

where

f_{wc} → denotes the mean compressive strength of the masonry (MPa);
f_b → denotes the mean compressive strength of the stones (MPa);
f_m → denotes the mean compressive strength of the mortar (MPa);
k_1 → factor depends on the bond between the stones and the mortar (=0.60 for rubble stones);
k_2 → factor depends on the type of masonry (=2.50 MPa for rubble stone masonry);
$\frac{V_m}{V_w}$ → denotes the ratio between the mortar and the masonry volume (≥0.30).

It is noted that, as extracting stones from the monument was not allowed, to test them in the laboratory, the rebound technique needed to be used in several locations. Calibration curves that are adequate for stones were used (e.g., [33]) to estimate the compressive strength of the stones. The scatter of the calculated values was quite significant. Thus, a conservative value of 50 MPa was adopted as the mean compressive strength of the stones.

Based on the in-lab tests on the mortar samples, the mean compressive strength of the mortar was estimated to vary between 2.0 MPa and 4.0 MPa [25]. The conservative value of 2.0 MPa was used to calculate the compressive strength of the rubble stone masonry of the spandrel walls. Finally, for the application of Equation (1), it is necessary to estimate the volume of mortar per unit volume of the masonry. This was performed for the spandrel walls in various regions of the bridge (Figure 17). This ratio was found to vary between 0.35 (in the regions closer to the arch) and 0.45 (away from the arch). For the sake of simplicity, an average value of V_m/V_w, equal to 0.40 was adopted.

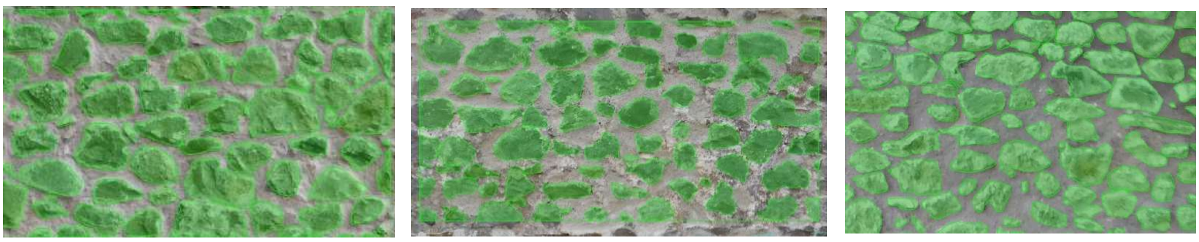

(**a**) (**b**) (**c**)

Figure 17. Calculation of stone area on the photogrammetric model for spandrel walls—construction with rubble stones: (**a**) upstream south area; (**b**) upstream north area; (**c**) downstream south area.

For the material filling the space between the spandrel walls, a value of compressive strength had to be assumed, as taking samples was not possible due to the constraints imposed by the Authorities for sampling the materials of monuments. Thus, the construction typology of the filling material was roughly estimated based on information gathered using a borescope [25]. Finally, a conservative value of the compressive strength equal to 0.80 MPa was adopted, calculated using Equation (1), assuming a mortar-to-stones ratio equal to 0.70, a compressive strength of the stones equal to 40 MPa and a compressive strength of the mortar equal to 0.70 MPa.

Estimating the modulus of elasticity of masonry is even more difficult than estimating its compressive strength as E-modulus values are extremely scattered [34]. For the needs of this numerical work, parameter analyses were performed for two values of the modulus of elasticity of the masonry, namely 600 and 1000 times the estimated compressive strength of the respective masonry typology, as shown in Table 1.

Finally, a laboratory examination of the samples taken in situ showed that the timber elements were made using the wood of Pinus Halepensis, a tree quite common in Mediterranean countries. The decayed state of the timber elements in the bridge did not allow for mechanical tests to be performed and for the mechanical properties of the wood to be evaluated. Thus, taking into account that in numerical calculations the timber elements are considered to be sound, a wood class C16 (according to [35]) was adopted. Thus, the compressive and the tensile strength of the timber were taken to equal 17 MPa and 10 MPa, respectively, whereas the E-modulus was taken to equal 8000 MPa.

4.2. Assumptions Related to the Foundation Soil

The bridge was assumed to rest on the foundation soil over the entire length and width of the abutments. The north abutment of the bridge is founded on solid limestone, whereas the south abutment is founded on limestone as well, presenting various degrees of disintegration, as boreholes in the region have shown (Figure 18 and [25]). The foundation soil is simulated by means of vertical surface elements of distributed elasticity, which can develop exclusively compressive stresses, while the modulus of subgrade reaction, k_v, for the numerical calculations, was estimated based on [36]. Thus, the values 40,000 MPa and 100,000 MPa were calculated for the south and the north abutment, respectively. Nonetheless, considering the uncertainties related to soil parameters and in order to study the effect of soil on the behaviour of the bridge, parameter analyses were performed for a range of values of the modulus of subgrade reaction, namely, k_v = 40,000 and 120,000 kN/m^2 for the south abutment; k_v = 100,000 and 300,000 kN/m^2 for the north abutment (Table 2).

Table 2. Combinations of moduli of elasticity of masonry and moduli of subgrade reaction accounted for in parameter analyses of the bridge.

Case	Modulus of Elasticity of Masonry (Regions 1 to 4) (MPa)	Modulus of Subgrade Reaction (Soft "S" or Medium "M" Soil) (kN/m^2)
I	min: E_1 = 8700, E_2 = 5350, E_3 = 1500, E_4 = 500	S: $K_{v,south}$ = 40,000, $K_{v,north}$ = 100,000
II	min: E_1 = 8700, E_2 = 5350, E_3 = 1500, E_4 = 500	M: $K_{v,south}$ = 120,000, $K_{v,north}$ = 300,000
III	max: E_1 = 14,500, E_2 = 8900, E_3 = 2500, E_4 = 800	S: $K_{v,south}$ = 40,000, $K_{v,north}$ = 100,000
IV	max: E_1 = 14,500, E_2 = 8900, E_3 = 2500, E_4 = 800	M: $K_{v,south}$ = 120,000, $K_{v,north}$ = 300,000

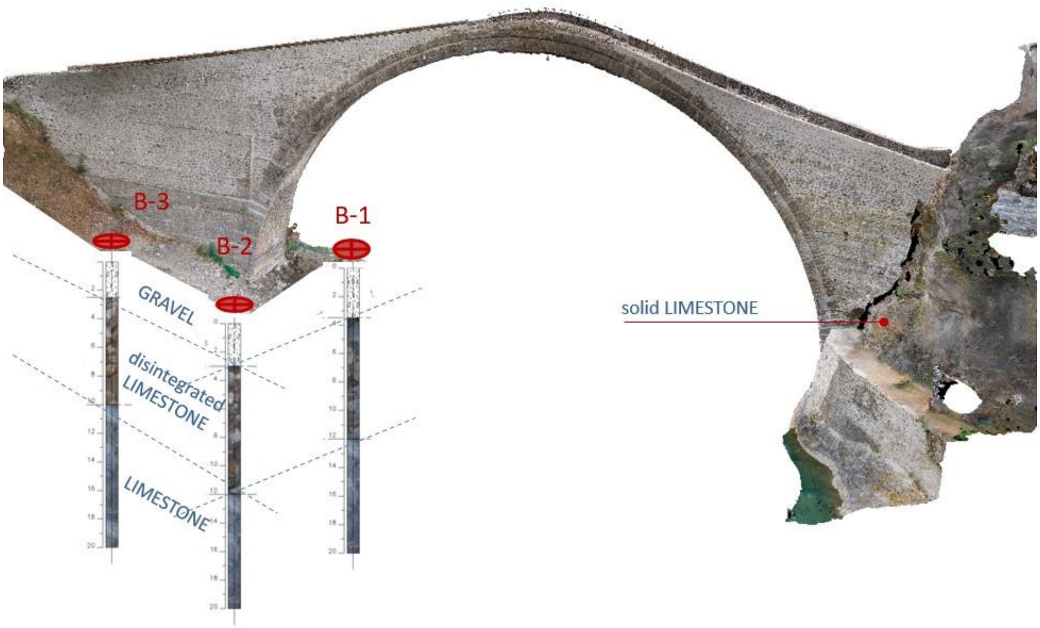

Figure 18. Upstream view of the bridge photogrammetric survey (Michaelidis [26]). The location of the geotechnical boreholes (B-1, B-2, B-3) and the respective findings are shown.

4.3. Timber Elements in the Abutments and in the Arch

As shown in Figure 5, horizontal and radial timber grids at intervals along the height of the abutments were found. The exact extent of the horizontal grids was not possible to identify, as some regions of the abutments were not safe for the personnel to reach. Therefore, the length of the timber grids included in the numerical model (Figure 19) is assumed to be the same for all of them. Furthermore, the timber grids are accounted for only in construction Phase 1 (see Table 3), comprising the abutments alone (before the completion of the arch). It is noted that preliminary analyses were performed on the model of the complete bridge. In those analyses, the timber elements were also included. However, as the results have proven the negligible contribution of the grids to the behaviour of the completed bridge, to simplify the numerical model, those elements were neglected in the subsequent calculations and replaced by the masonry of the mechanical properties allotted to the relevant construction typology. This choice is justified by the following considerations: (a) when examining the completed bridge at its as-built state (Phase 2), as well as after the 1913 explosion (Phase 3), it is reasonable to assume that the timber elements were still sound, although deprived of a structural function, and (b) the replacement of the disintegrated timber elements in the framework of the rehabilitation of the bridge is not feasible, and the holes in their locations will be filled with a mortar of adequate mix proportions.

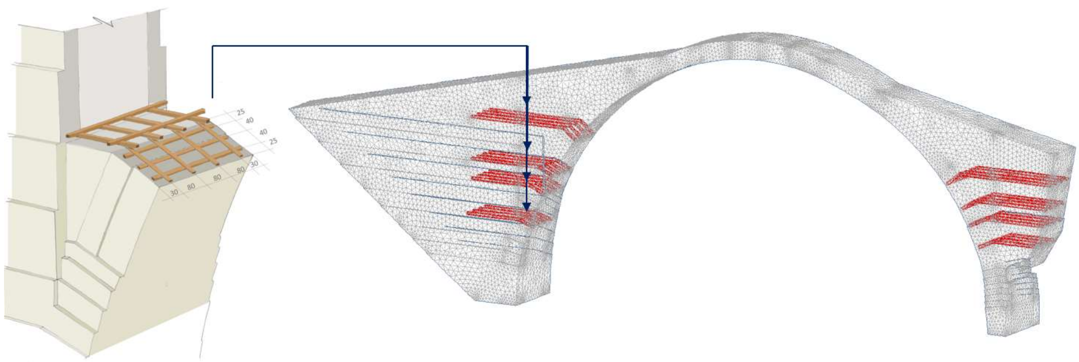

Figure 19. Bridge model including the timber grids.

Table 3. Phases considered in the investigation of the structural behaviour of the bridge.

Phase	Description—Structural Model	Documentation Reference
Phase 1	Construction phase: construction of abutments 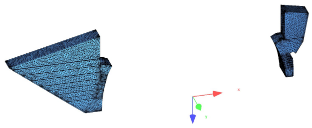	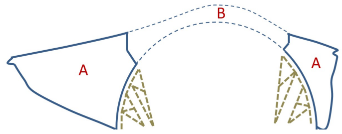 (*)
Phase 2	Construction phase: construction of the central region of the arch. Bridge completed. 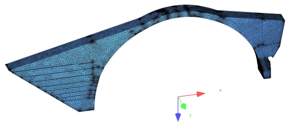	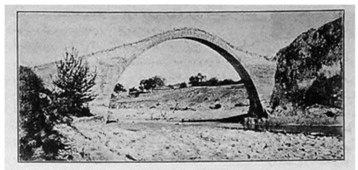 The bridge at the beginning of the 20th century (**)
Phase 3	Damaged bridge (1913) 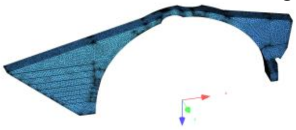 	 Rhomaides-Zeitz, 1913 [29]
Phase 4	Repaired bridge (1913) 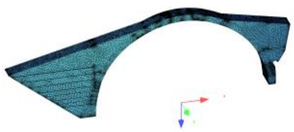 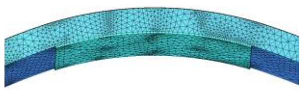	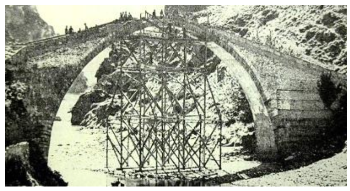 Fr. Boissonnas, 1913 [37]  RC jacket is shown in its current state

(*) Sketch showing the segmental construction of abutments as described in Section 2. (**) Photo by unknown photographer (Courtesy V.Kaskanis).

Finally, as it was documented that the parapets of the bridge, made of masonry, are not connected to the spandrel walls, they are not included in the numerical model. Their self-weight is, however, added to the permanent loads of the bridge.

5. Documentation-Based Calculation Methodology

Before describing the methodology adopted for the numerical calculations and before presenting the key numerical results, some comments are needed to justify the options made for the work presented herein. One of the major criteria for the acceptance of the results of the numerical calculations, internationally recognised [38] and required by competent Authorities in Greece [39], is their ability to verify the pathology observed in the monument at its current state. If this criterion is fulfilled, the numerical model and the adopted methodology may be considered credible and used in the subsequent stage, that of investigation of the efficiency of alternative intervention schemes. To check compliance with this criterion, preliminary elastic analyses were performed, considering the complete bridge, allocating though to the various regions of masonry the mechanical properties documented at the present time. In those preliminary analyses, the self-weight of the bridge was the only load on the structure. The results of those analyses have led to two major conclusions, namely, (a) the compressive stresses developing throughout the bridge due to its self-weight are small compared to the compressive strength estimated for all regions of different construction typologies. Indeed, the maximum principal compressive stresses occur in the arch (Figure 20a), and they nowhere exceed 1.88 MPa, i.e., 20% of the estimated compressive strength of the arch. Similarly, the maximum stress value in the spandrel walls is equal to 0.35 MPa, i.e., approximately 15% of the estimated compressive strength of the area. And (b), in Figure 20b, one can see two regions where high tensile stresses occur (0.88 MPa and 1.25 MPa, respectively), largely exceeding the tensile strength of the masonry. Therefore, one would expect damage in those regions. As shown in Figure 21, the area at the intrados is free of damage, whereas no cracks were observed at the extrados of the arch. This major discrepancy between the surveyed damage and the numerical results was attributed mainly to the fact that the vertical deformations of the abutments (due to their self-weight) induce large deformations to the arch connecting them and, hence, high stresses. Nonetheless, it is reasonable to assume that a significant part of those deformations took place before the completion of the arch, in the course of some months, when the abutments were free-standing. It was, therefore, decided to examine the state of stresses and deformations of the bridge, considering the major phases of its construction and the events that have occurred during its lifetime. On the other hand, as the compressive stresses developing in the bridge are small compared to the strength of the masonry and, seemingly within the elastic range under vertical loads, the decision was made to perform elastic analyses. This option was also supported by the lack of reliable information related to the inelastic behaviour of the various masonry typologies, in terms of resistances and—mainly—deformation properties. Additionally, the decision was made to perform parametric analyses (as per Table 2), to consider the effect of the uncertainties related to the estimated moduli of elasticity and to the soil parameters.

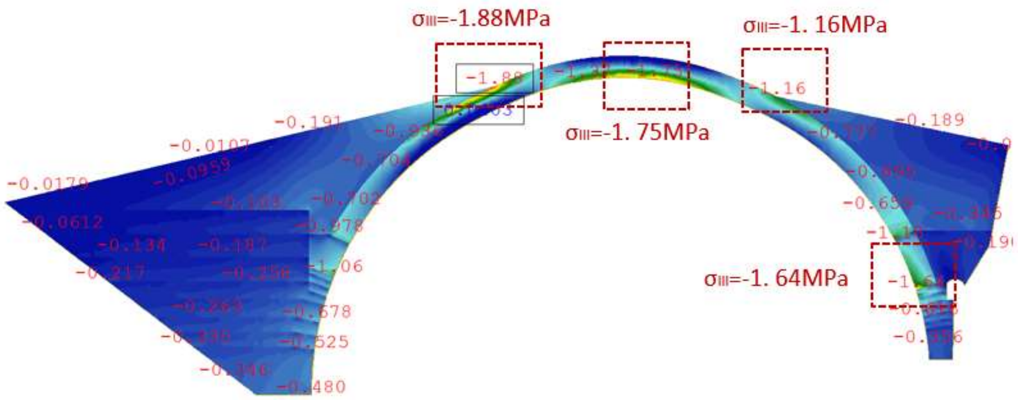

(**a**)

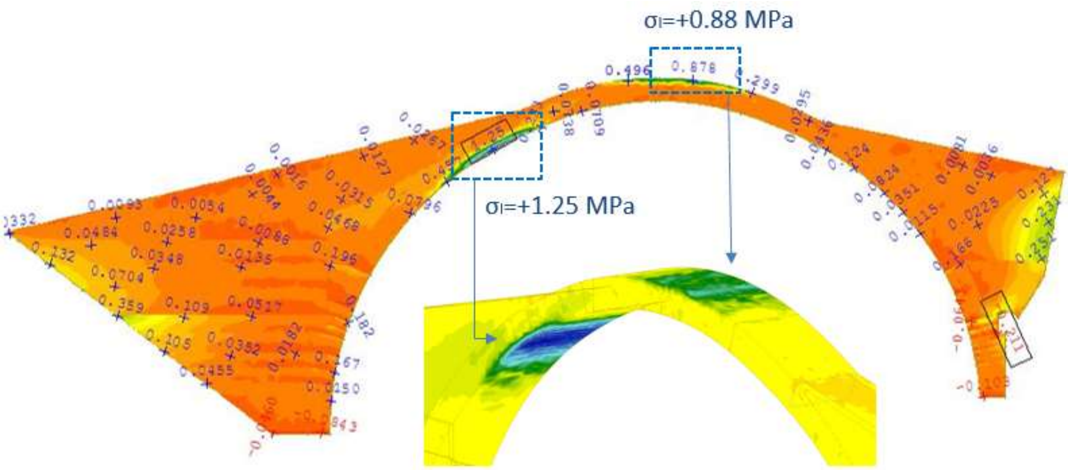

(**b**)

Figure 20. Principal stress contours: (**a**) compressive stresses; (**b**) tensile stresses.

Figure 21. The area of high tensile stresses (in green and blue, calculated by analysis considering the complete bridge). The region (intrados of the bridge) is free of damage. The highly stressed area at the extrados roughly coincides with the region damaged due to the 1913 explosion which was replaced by concrete.

The Bridge under Its Self-Weight-Phases Considered in Calculations

For each examined phase of the bridge, the stresses and deformations are calculated, and they are adequately combined with those calculated for the previous phase(s). In this part of the numerical work, only the self-weight of the respective portions of the bridge is considered. It is noted that the live loads (the weight of pedestrians and—originally—of mules transporting goods) are neglected, as they are minimal compared to the self-weight of the bridge. The examined phases are listed in Table 3 and described herein:

Phase 1—Construction of the abutments: This phase comprises the construction of the abutments and part of the arch up to an angle of 30° from the springing line. This phase is documented by (a) the lack of signs of a general scaffold of the bridge [25] and (b) the similarities with the Plaka bridge [28]. The construction of the abutments takes most of the entire construction time of a single-arch bridge. Thus, if the construction is completed in one year (summer and early fall), the abutments remain free-standing for some months. If the construction is completed within a two-year period, the free-standing period of the abutments exceeds one year. In either case, the elastic deformations of the massive abutments, as well as of the foundation soil, take place before the construction of the central region of the arch. For the Konitsa bridge, there are two additional characteristics justifying the consideration of Phase 1, namely, the different soil conditions on the two banks of the river and the pronounced geometrical asymmetry of the two abutments (Figure 18), with the larger abutment (the south one) being founded on disintegrated limestone. Thus, significant differential settlements are expected at the foundation level of the two abutments. Nonetheless, a portion of the differential settlements, occurring before the construction of the central region of the arch, are not expected to affect the behaviour of the bridge after its completion. This is indeed confirmed by the results of the calculations presented in Section 6.1. It is noted that this is the only phase at which the timber grids are introduced in the numerical model, with their identified original geometrical properties, although at the current stage, they are disintegrated.

Phase 2—Construction of the central region of the arch (bridge completed): The scaffold and formwork are installed in the river and the central region of the arch is constructed. This phase of the completed bridge is valid until the 1913 explosion.

Phase 3—Immediately after the 1913 explosion: The portions of the arch lost due to the explosion, as documented in situ by the limits of the plain concrete cast to fill them, are removed from the numerical model and the stresses and deformations are recalculated. The dynamic phenomenon of the explosion is not simulated, though. The bridge is examined after the event, under its self-weight alone, for the purpose of interpreting the observed cracks, as well as its survival, despite the loss of extensive portions of the arch.

Phase 4—After Rehabilitation: In this phase, the missing parts of the arch are filled with plain concrete and the RC jacket at the intrados is constructed. It should be mentioned that for this phase, the intrados RC jacket was considered to be in good condition, as it was at the time of its construction. It is noted that the added concrete (both at the extrados and at the intrados) contributes to the stiffness of the bridge only for live loads and accidental actions. When stresses and deformations due to the self-weight of the bridge are calculated, only the self-weight of the repair concrete is accounted for. This is because the repair took place without any temporary shoring of the bridge, as documented by the historical photographs (e.g., Figure 6b), in war conditions. On the contrary, the added plain and reinforced concrete do contribute to the resistance of the bridge when additional vertical loads (such as live loads of practically negligible value compared to the self-weight of the bridge), seismic actions or floods are accounted for.

6. The Structural Behaviour of the Bridge—The Effect of the Examined Phases

Since the volume of the numerical results is rather large, due to the phase-by-phase calculations and the performed parametric analyses, only selected results are presented herein, especially those permitting us to interpret the structural behaviour of the bridge, including the observed pathology and those leading to decisions regarding the interventions to the monument. For this purpose, the results are presented in the form of deformations and principal (compressive and tensile) stresses, while relevant comments are offered herein.

6.1. Phase 1—Construction of Abutments and Portions of the Arch

During Phase 1, the maximum vertical deformation occurs at the south abutment (Figure 22), both because of the larger mass of this abutment and because of the softer soil on the south bank of the river. For the most adverse combination of moduli of elasticity and soil characteristics (case I in Table 2), a difference of 8 mm in the vertical deformations at the base of the two abutments was calculated [40]. This difference, due to the elastic vertical deformations of the abutments, as well as due to the different soil conditions, did not affect the overall behaviour of the completed bridge as it occurred at the stage where the abutments were free-standing and independent from one another. Thus, as explained in Section 6.2, those deformations are not added to those calculated for the completed bridge. For this first phase, the values of principal compressive and tensile stresses are small (a maximum principal compressive stress equal to 1.30 MPa and a maximum principal tensile stress equal to 0.10 MPa).

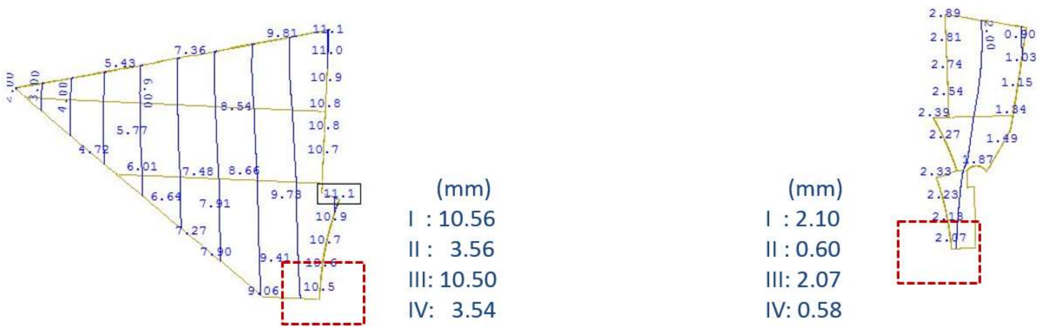

Figure 22. Elastic vertical deformations for Phase 1 for the four examined cases (as per Table 2).

6.2. Phase 2—Construction of the Central Region of the Arch (Bridge Completed)

Figure 23 shows (in red) the vertical deformations calculated considering the self-weight of the entire bridge, i.e., without accounting for the intermediate Phase 1 for the most adverse combination of moduli of elasticity and moduli of subgrade reaction (Case I in Table 2). In the same Figure 23, one can see (in blue) the vertical deformations calculated in Phase 2, after the subtraction of the deformations effectuated in Phase 1, assumed not to affect the overall behaviour of the bridge. The deformations are shown for the most critical locations, namely, at the base of the abutments and at the connection of the central region of the arch to the abutments. When the construction phases are considered, there is a difference of 2.25 mm (Figure 23, blue values) in the vertical deformations at the base of the two abutments for the most adverse combination of moduli of elasticity and soil properties (Case I in Table 2). On the contrary, if the completed bridge is considered, without the intermediate stage (Phase 1), the difference in vertical deformations of the two abutments rises to 10.23 mm (Figure 23, red values). This observation is valid not only for the deformations at the base of the abutments but also for the most critical regions of the bridge, namely, at the locations where the arch is joined to the two abutments (Figure 23).

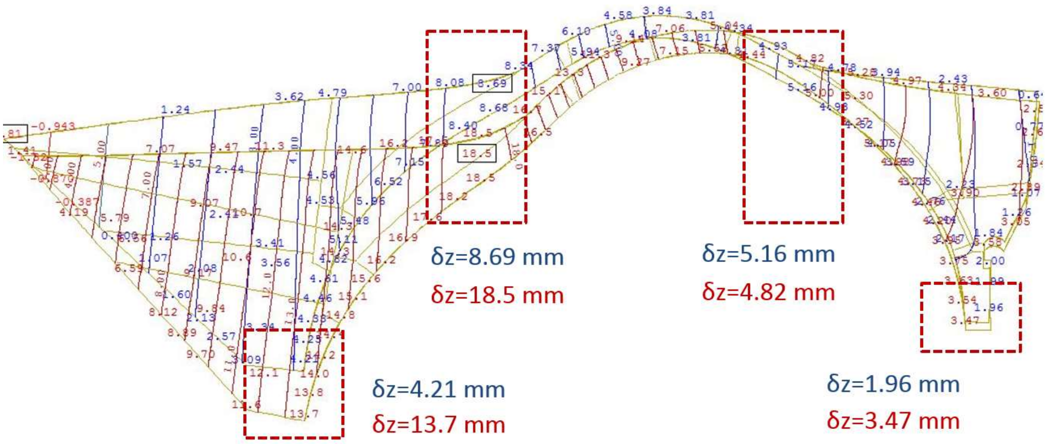

Figure 23. Elastic vertical deformations. Blue numbers show the deformations calculated for Phase 2 alone (by neglecting the deformations of Phase 1), while red numbers show the deformations calculated for the complete bridge, without accounting for construction phases.

Looking at the stresses developed in Phase 2, it is observed that the principal tensile stresses at the most stressed region (where the arch is joined to the south abutment), reach only locally a value of +0.32 MPa (Figure 24) for the most adverse combination of moduli of elasticity and soil characteristics (Case III, Table 2). The range of the calculated tensile stresses seems to be compatible with the lack of damage in the critical region at the intrados of the bridge (Figure 21). On the contrary, as shown in the same Figure 21, if the construction phases are not considered, very high tensile stresses are calculated, far beyond the tensile strength of the masonry in the region. Regarding the principal compressive stresses, it is observed that for the most adverse scenario (Case III, Table 2), they reach a value of 2.01 MPa (Figure 25). The regions where the highest compressive stresses develop coincide with the strongest areas of the bridge, i.e., the abutments and the arch, of estimated compressive strength equal to 14.50 MPa and 8.90 MPa, respectively (Table 1).

At this point, it is appropriate to mention that the performed calculations prove (Figures 23–25) that the most critical region of the bridge is not the crown of the arch, as is typically the case in arch bridges, but the region where the arch is joined to the south abutment. This is obviously due to the pronounced geometrical asymmetry of the bridge, with the south abutment being massive and stiff and, thus, providing full fixity of the arch. Although no simulation of the dynamic phenomenon of the explosion was attempted, it is sensible to assume that the bridge survived because the explosives were located in the region of the crown of the arch, which is definitely not the critical area of this bridge.

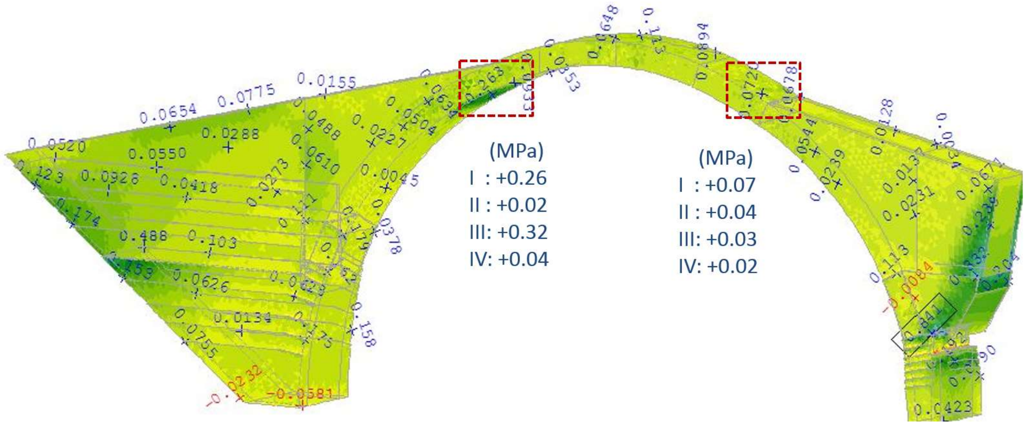

Figure 24. Principal tensile stresses for Phase 2 (Table 3).

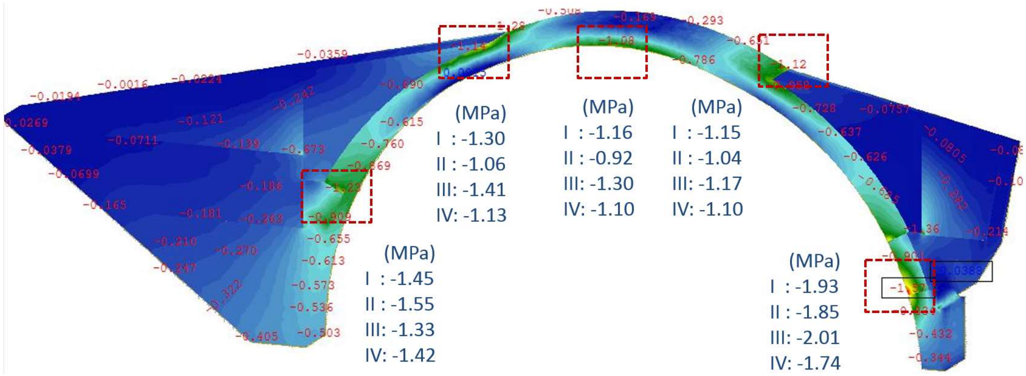

Figure 25. Principal compressive stresses for Phase 2 (Table 3).

Another finding of the calculations for Phases 1 and 2 is related to the structural role of the horizontal timber grids identified in the two abutments. As shown in Figure 26, during Phase 1, i.e., when the abutments were free-standing before the completion of the arch, the timber elements were in tension (Figure 26a), functioning as reinforcement of the two abutments behaving as cantilevers. On the contrary, when the bridge was completed (Phase 2), the axial forces in the timber grids were compressive (Figure 26b). In either construction phase, the values of axial forces are much smaller than those corresponding to the strength of the wood.

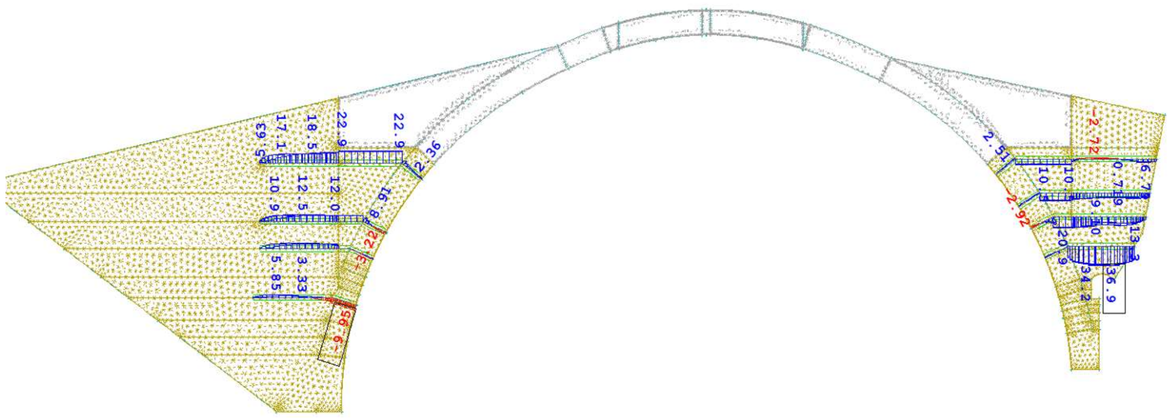

(**a**)

Figure 26. *Cont*.

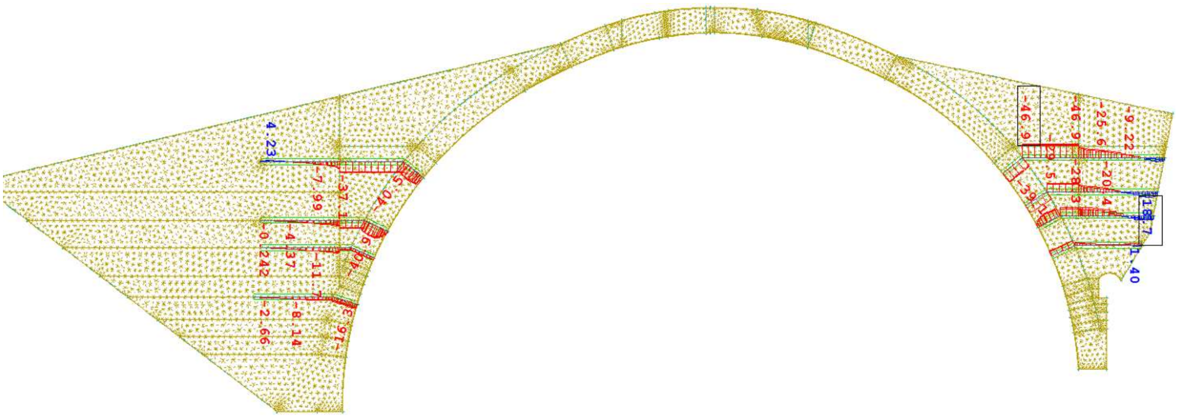

(**b**)

Figure 26. Axial forces in the timber elements (in kN). Tension forces are in blue, compression forces are in red. Timber elements are indicated in green, (**a**) Phase 1—construction of the abutments, and (**b**) Phase 2—after the bridge is completed.

6.3. Phase 3—Damage Due to Explosion (1913)

After the explosion (Phase 3), the significant loss of material in the region of the crown of the arch and the resulting reduction in stiffness leads to small additional vertical deformations (Figure 27). An uplift of limited value is observed in the region of the crown of the arch. As expected, based on the kinematics of the damaged region, a rotation occurred with respect to the crown of the arch, resulting in horizontal deformations (perpendicular to the longitudinal axis of the bridge, Figure 28) [40]. The out-of-plane deformation of the arch due to the explosion leads to additional compressive stresses in the downstream corner of the S-abutment and the upstream corner of the N-abutment (as illustrated in Figure 28). On the contrary, additional tensile stresses occur in the upstream corner of the S-abutment and in the downstream corner of the N-abutment. Thus, as shown in Figure 28, the results of the numerical calculations do interpret the damage observed in the abutments, attributed to the explosion.

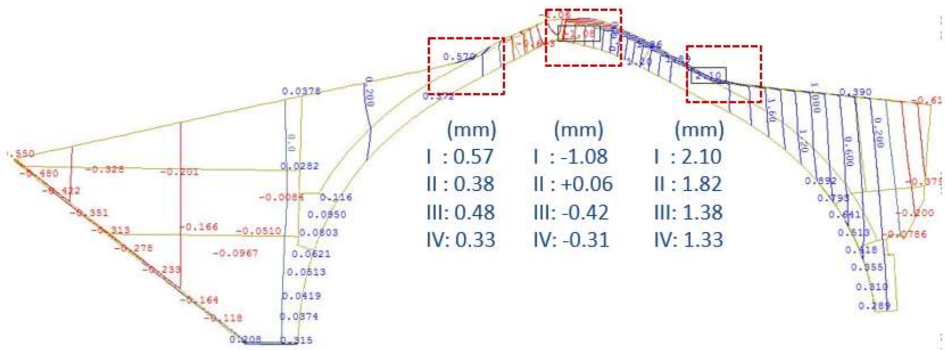

Figure 27. Phase 3—additional vertical deformations due to the loss of mass caused by the explosion.

Furthermore, principal tensile stresses of high values are observed in the damaged area (Figure 29a). The loss of material due to the 1913 explosion caused a significant increase in the principal compressive stresses in the damaged arch (Figure 29b). Indeed, the maximum principal compressive stress reaches the value of 6.32 MPa, with the compressive strength of the arch estimated at 8.90 MPa. It is noted that the performed elastic analyses do not account for the effect of creep that would definitely worsen the state of the damaged bridge. It is, therefore, believed that the immediate intervention of the engineers of the French Army has saved the bridge from the collapse of its arch at least.

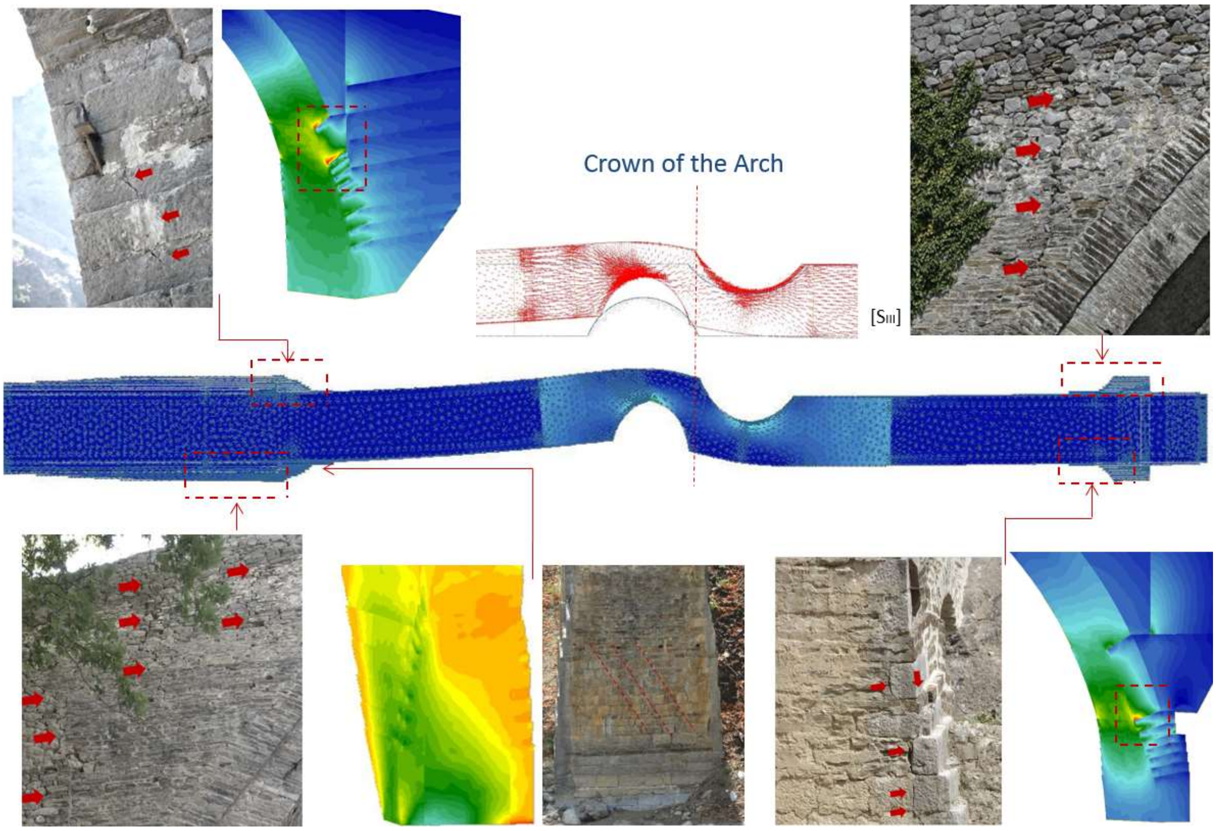

Figure 28. Phase 3—interpretation of pathology, outside the damaged region of the arch.

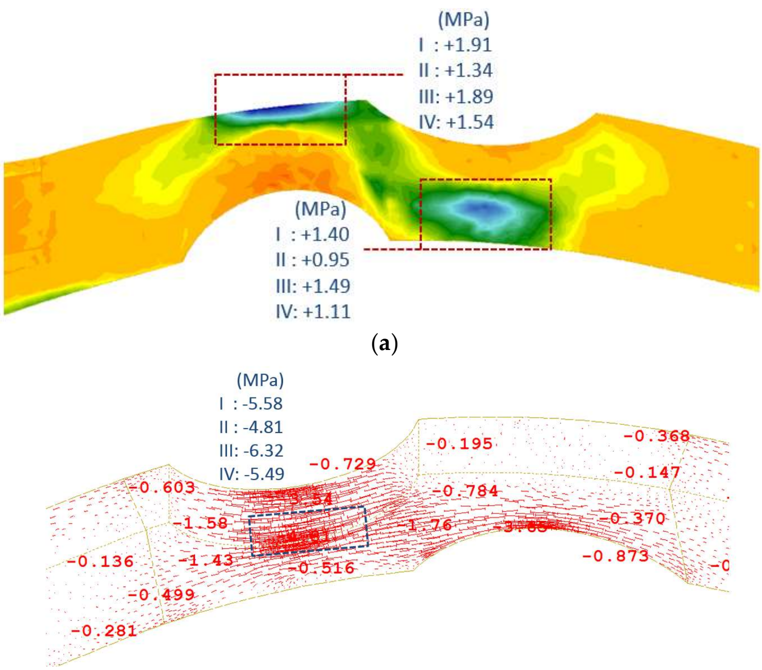

Figure 29. Principal stress contours in the damaged area of the arch: (**a**) principal tensile stresses (extrados); (**b**) principal compressive stresses (intrados).

6.4. Phase 4—Repair of the Bridge (1913)

The filling of the damaged areas with concrete reinstated the integrity of the arch. Nonetheless, the deformations caused by the explosion are obviously permanent. Furthermore, as the repair of the arch was carried out without temporary shoring (Figure 6b), the added concrete (plain or reinforced) constitutes an additional self-weight. Actually, Figure 30 shows that the added concrete has caused a further vertical deformation at the crown of the arch, of limited value, though. Furthermore, Figure 31 shows a small decrease in the principal compressive stresses in the area affected by the explosion (comp. with Figure 29).

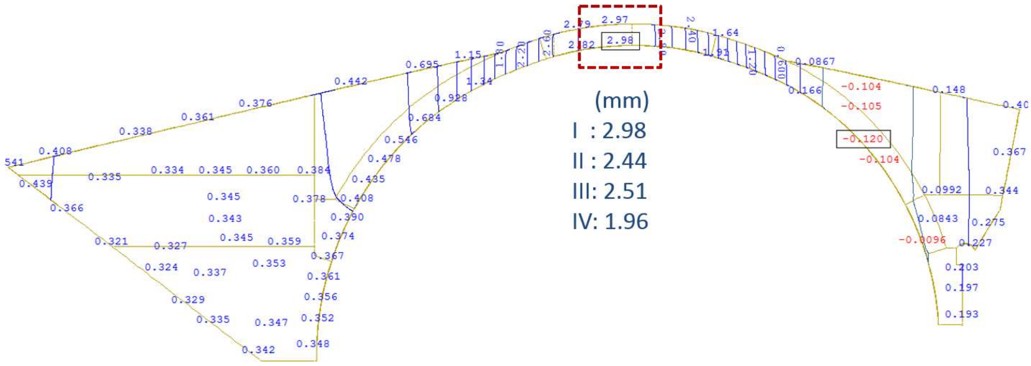

Figure 30. Phase 4—additional vertical deformations after the 1913 repair of the arch.

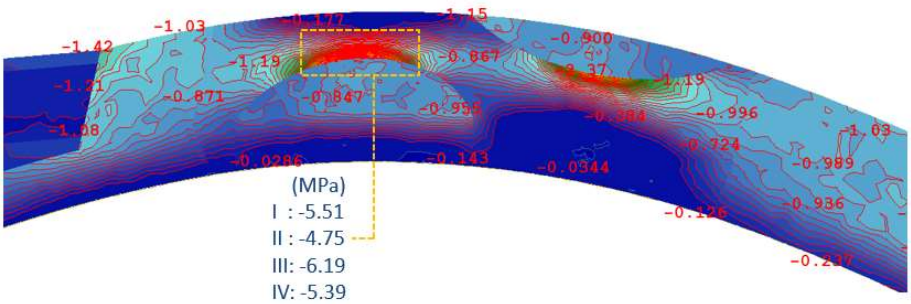

Figure 31. Phase 4—principal compressive stresses at the crown of the arch area after the 1913 repair.

7. The Structural Role of the RC Jacket at the Intrados of the Arch

The phase-by-phase methodology has allowed for the structural behaviour of the bridge to be understood, for the observed pathology to be qualitatively interpreted and for the safety of the bridge under its self-weight to be confirmed. Furthermore, undoubtedly, the reinstatement of the integrity of the arch thanks to its repair was necessary. On the other hand, as the RC jacket at the intrados of the arch does not contribute to the arch action under vertical loads, it is reasonable to assume that the purpose of this intervention was to strengthen the arch against actions involving the out-of-plane behaviour of the bridge, namely, floods and earthquakes. This aspect is examined in this section.

7.1. The Influence of Flow Pressures

Within the project, a hydraulic study was performed [36] with the purpose of calculating the water level in the river for floods with various return periods, as well as the respective flow pressures.

The hydraulic study for the region affecting the bridge of Konitsa has proven that the flow characteristics of the Aoos River are rather mild. The respective numerical calculations have confirmed the non-criticality of the flow pressures for the bridge. As an indication, it is mentioned that the flood scenario with return period T = 100 years includes only a small part of the base of the south abutment (Figure 32a).

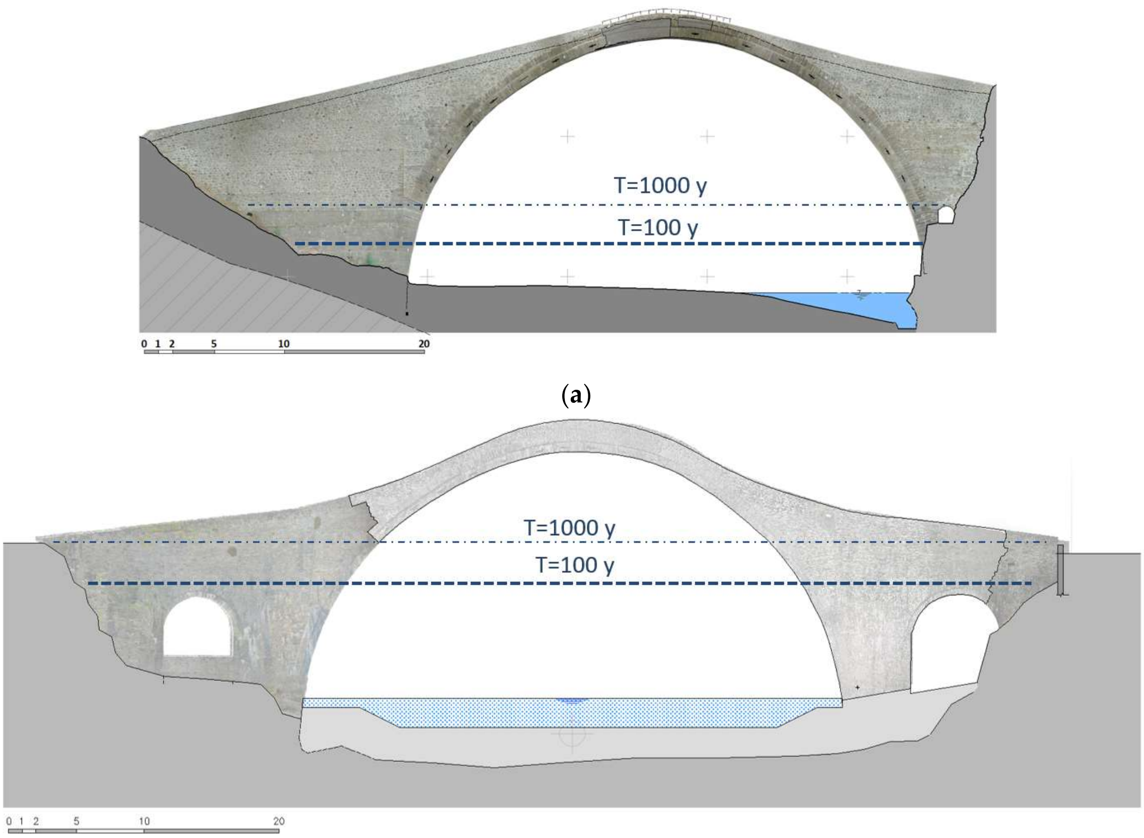

(**a**)

(**b**)

Figure 32. Highest flow level for flood scenarios, return periods T = 100 years and T = 1000 years: (**a**) Konitsa bridge (1869), Aoos River; (**b**) Plaka bridge (1866), Arachtos River.

It is noted that the bridge constructors of Epirus were very experienced and, before making decisions about the location and the geometry of the bridge to be constructed, they studied the hydraulic conditions of the area as well. This is confirmed by the design of the bridge of Konitsa, where relief arches are not provided. The small opening in the north abutment (Figure 32a) was formed a few decades ago for irrigation purposes. On the contrary, in the bridge of Plaka (built three years earlier in 1866), the same constructors have provided two relief arches (Figure 32b), being aware—by observation—of the much more unfavorable hydraulic characteristics of the Arachtos River [41].

Based on this investigation, one may conclude that the RC jacket at the intrados of the bridge is not needed for protection against flood. Nonetheless, as the hasty intervention, in war conditions, was performed by engineers who were not acquainted with the climatic conditions of the area, one could assume that they have tried to strengthen the vulnerable region of the crown of the arch against flood. To check this hypothesis, numerical calculations were performed, accounting for the extreme 1000-year flood scenario.

Out of all the performed parametric calculations, listed in Table 2, the results of the most adverse case (Case I) are presented herein. In Case I, all types of masonry are accounted for with the smallest value of E-modulus, while soft soil conditions are assumed. The flow pressures are first imposed on the repaired bridge by excluding the RC jacket at the intrados from the model. This calculation shows that tensile stresses as high as 0.707 MPa (Figure 33a) develop at the interface between the arch and the plain concrete at the intrados, indicating the detachment of the two components. Afterward, another calculation was performed. In this case, the plain concrete added to repair the arch was excluded, while the RC jacket at the intrados was added to the model. This calculation shows tensile stresses (with a maximum value of 4.10 MPa—Figure 33b) and compressive stresses (with a maximum value of 9.0 MPa) developing in the RC jacket. These results prove, be it in a qualitative way, the need for the RC jacket.

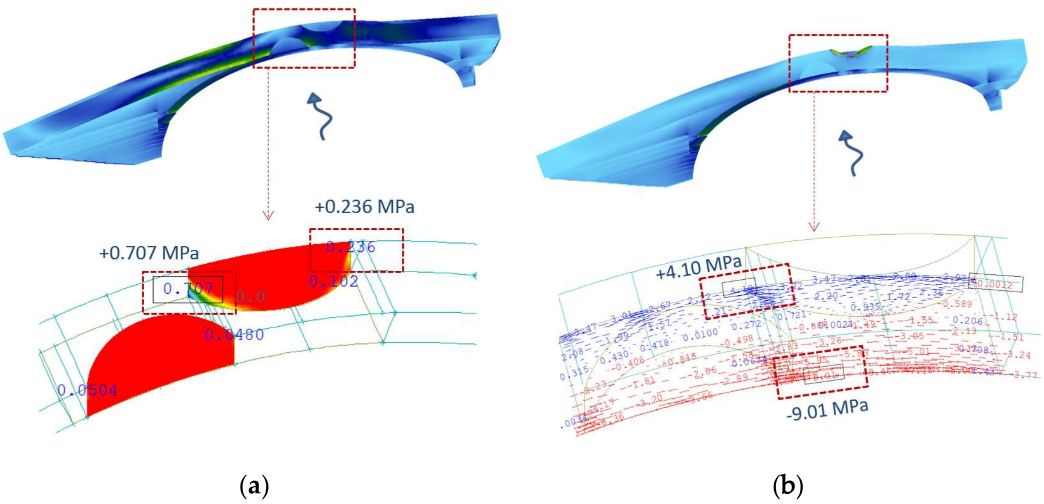

Figure 33. Results of numerical calculations for the damaged region of the bridge. Flow pressure for the 1000-year flood scenario. Principal stresses (**a**) when the RC jacket at the intrados is not included in the model, and (**b**) when the RC jacket is considered, while the portion of the plain concrete at the extrados being subjected to tension (as per Figure 33a) is not included in the numerical model.

7.2. The Influence of Earthquakes

The bridge is situated in the least seismically active region of Greece, as also evidenced by the map of Figure 34 [42] and recognised by the current Seismic Code [43], classifying the municipality of Konitsa in the lowest seismic zone of the country.

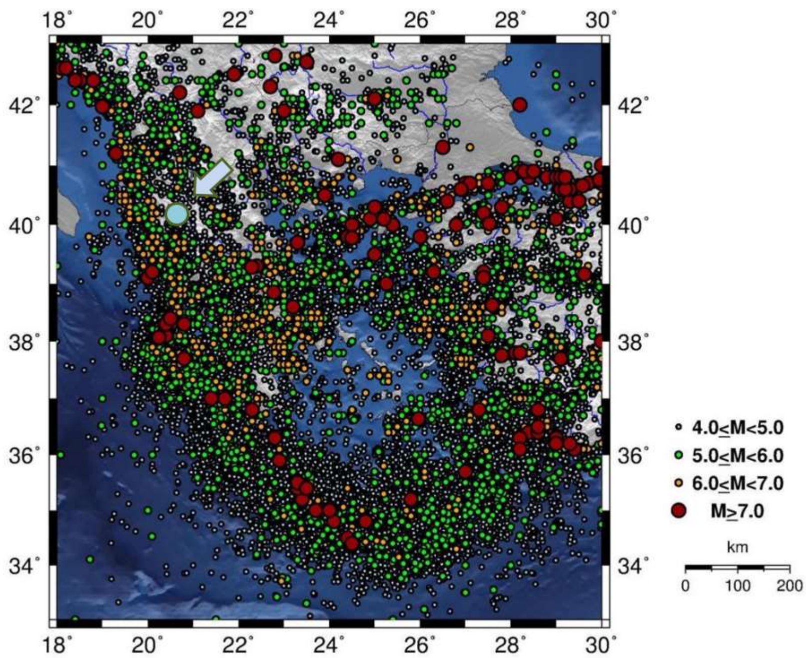

Figure 34. Epicenters of shallow earthquakes in Greece of magnitude M > 4 that occurred between 550BC and 2018AD [42]. The light blue circle shows the location of the bridge of Konitsa.

In the lifetime of the bridge, within its area, seismic events of magnitude M > 5 occurred, according to [42], namely, 22 December 1919 (estimated magnitude M6.3), 26 July 1996 (magnitude M5.2) and 6 August 1996 (magnitude M5.6), all of them with an epicentral distance not exceeding 15 km. Although there is no source mentioning any damage to the bridge caused by those or other earthquakes, one may not exclude that minor damage might have occurred that was not meticulously surveyed.

Before presenting the results of the numerical calculations related to the seismic behaviour of the bridge, the following clarifications are needed: (a) As the bridge is listed by the Ministry of Culture, interventions that may enhance the seismic capacity and, simultaneously, affect the heritage value of the bridge are not allowed. Therefore, an increase in the design seismic action, e.g., to account for the importance of the bridge, was not considered; (b) according to the Authorities, this study should examine the possibility of removing the RC jacket at the intrados of the arch, thus, giving the bridge its original shape; and (c) in case the study proves that the RC jacket is to remain, it should be checked that its original sectional dimensions and reinforcement are sufficient for the bridge to sustain the conventional seismic action, without any increase (as per (a)). Taking all those constraints into account, the following numerical calculations were performed:

(a) Eigenvalue analysis, with the purpose of qualitatively identifying the most critical modes for the seismic behaviour of the bridge. To this purpose, the as-built bridge is modelled, before the 1913 damage. The results of this analysis are shown in Figure 35, where the modes with the most significant contribution are presented. The results show that the most critical direction is the transverse one, out-of-plane of the bridge, with the contribution factor of the translational first mode being close to 50%. This is the reason why only results concerning the seismic action in the transverse direction are presented herein. This is more so because the effect of the RC jacket at the intrados is investigated;
(b) Equivalent static analysis for the conventional seismic action resulting from the current Seismic Code, assuming a q-factor equal to unity. The conventional seismic action is imposed on the numerical model representing the repaired bridge, excluding the RC jacket. The results, presented in Figure 36, show that the tensile stresses developing in the damaged and, subsequently, repaired region of the arch are by far larger than any value that could be assumed for the bond between the arch and the added plain concrete. This proves that the RC jacket at the intrados, thanks to its longitudinal reinforcement, is needed to undertake the tension due to the transverse action of an earthquake. It seems that, on the contrary, the developed compressive stresses can be resisted by both the arch and the plain concrete. Another interesting, although qualitative result, is related to the tensile and compressive stresses calculated at the base of the two abutments. As shown in Figure 36, the tensile or compressive stresses develop in the same face of the two abutments. This is an observation that confirms the interpretation of the damage (presented in Section 6.3), attributed to the 1913 explosion. The numerical values of the compressive stresses at the base of the abutments are significantly smaller than the compressive strength of the masonry (=14.50 MPa, Table 1), while the tensile stresses seem to be far beyond the tensile strength of the mortar. Nonetheless, as shown in Figure 37, the peak tensile stresses occur in the smaller dimensions section of the north abutment, while they are very much localised;
(c) Although the purpose of the numerical calculations considering the seismic action was neither to design the bridge nor to upgrade its seismic resistance, the results show that some damage is to be expected under the design earthquake;
(d) In conclusion, the results of the numerical analyses, although oversimplified, allow for the structural function of the RC jacket to be qualitatively identified. As shown in Figure 38, during a seismic event, the portion of the unreinforced concrete at the extrados of the arch subjected to compression collaborates with the masonry arch, whereas the concrete portion belonging to the tensioned zone of the section risks being detached from the masonry arch. Therefore, it is sensible to assume that the RC jacket, thanks to its reinforcement, can prevent the occurrence of cracks in the tensioned zone or keep their openings to an acceptable value.

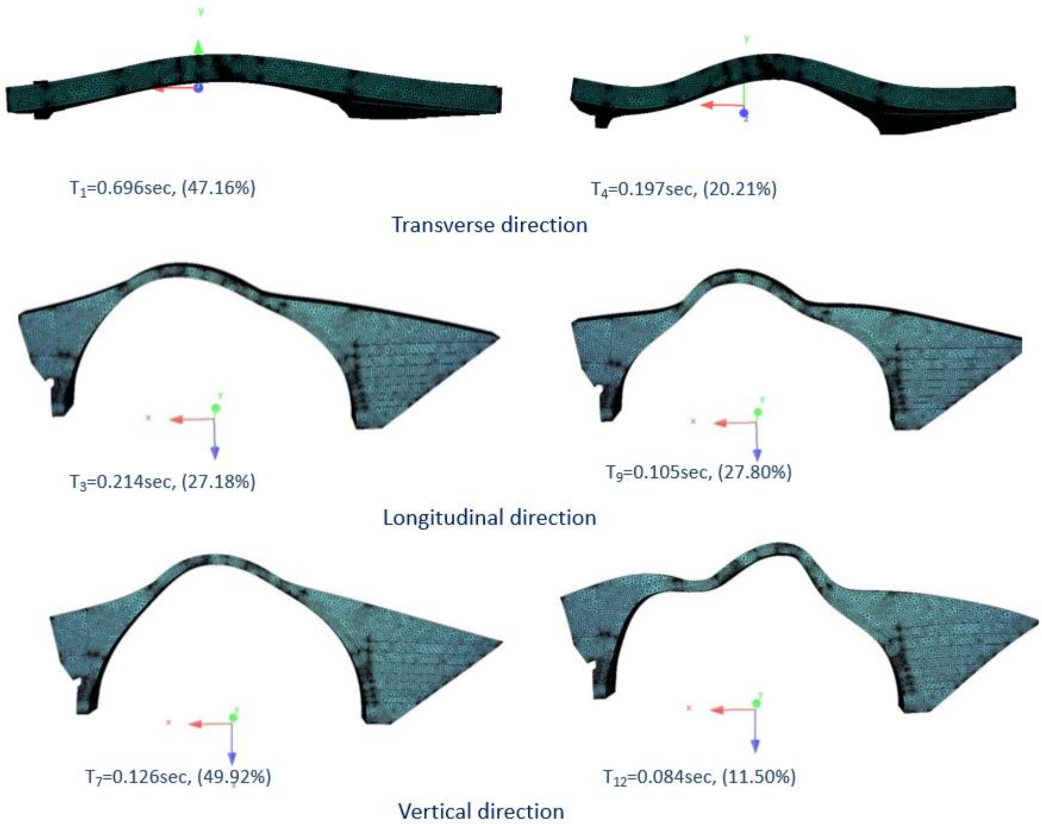

Figure 35. Modal shapes of the bridge, in the longitudinal, transverse and vertical directions. Only shapes presenting contribution factor larger than 10% are shown.

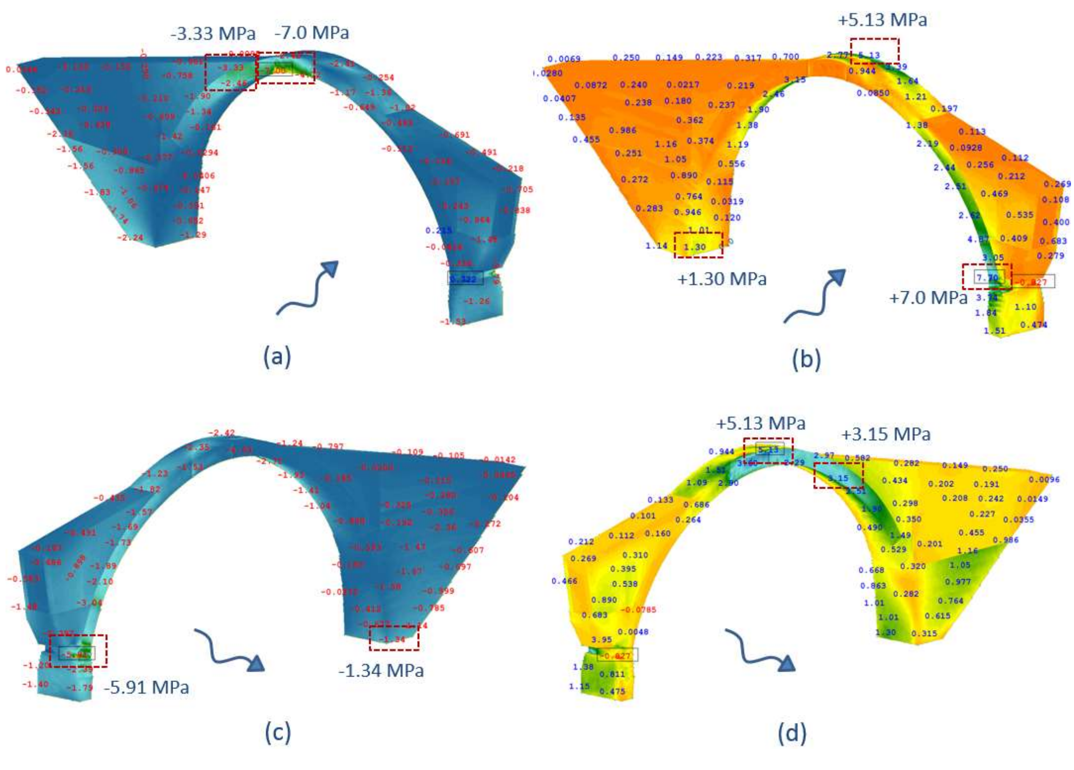

Figure 36. Principal stresses due to the seismic action in the transverse direction: (**a**) upstream face—compressive stresses; (**b**) upstream face—tensile stresses; (**c**) downstream face—compressive stresses; and (**d**) downstream face—tensile stresses.

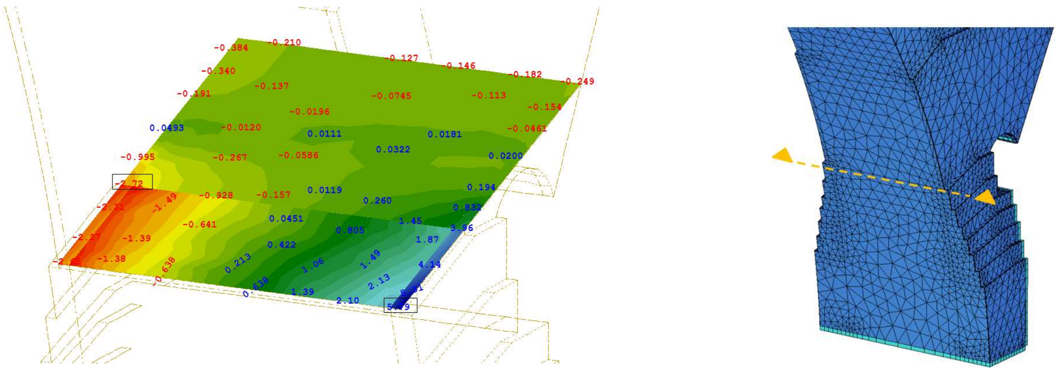

(**a**) (**b**)

Figure 37. (**a**) Distribution of principal tensile stresses at the base of the north abutment, at the level indicated in (**b**).

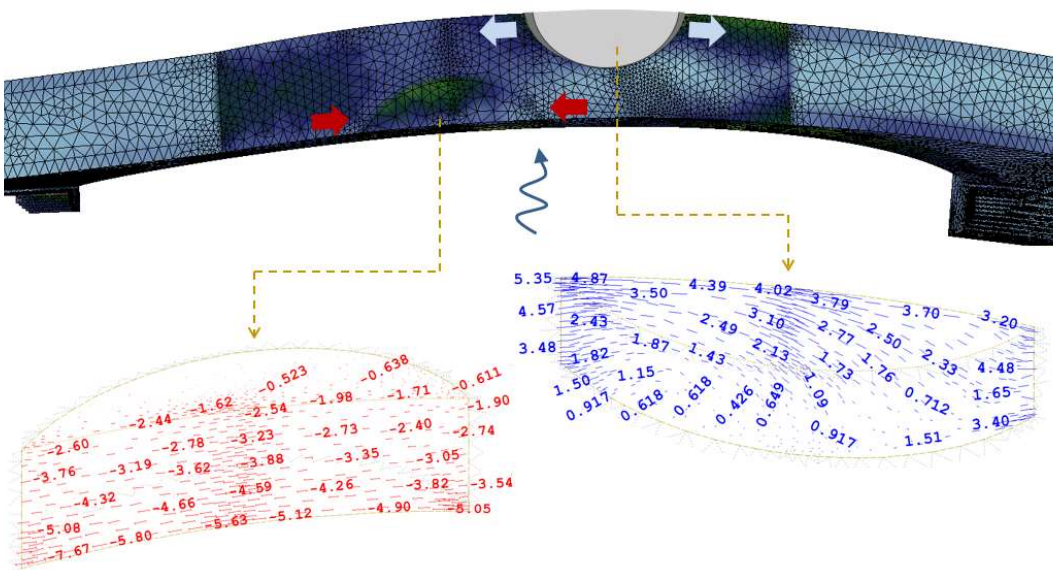

Figure 38. Principal stresses developing in the plain concrete at the extrados of the bridge under the seismic action in the transverse direction.

7.3. Rehabilitation Measures

Based on the exhaustive documentation of the bridge [25], as well as on the numerical calculations presented in this paper, a scheme of interventions was proposed and unanimously approved by the competent Central Council of the Ministry of Culture. The proposed interventions do not alter either the morphological characteristics of the bridge or its structural behaviour. On the contrary, they contribute to the preservation of its values, while providing the necessary protection against expected actions. More specifically, the main intervention to be applied is that of the reconstruction of the RC jacket at the intrados of the bridge. This intervention was approved both because the respective need was proven and because the RC jacket constitutes part of the history of the monument. Nonetheless, for its reconstruction, materials of improved quality are used, namely a C35/45 (XC4) concrete and stainless steel (EN1.4301 (AISI 304), category InE500). Considering those materials, adequate calculations have proven that the original characteristics of the jacket, i.e., its extent, its thickness and its reinforcement ratio, are sufficient to resist the out-of-plane actions specified by the authorities.

Other measures that were proposed and approved are, for example, the repair of the surveyed cracks using grout and the protection of the plain concrete at the extrados of the arch (using a thin layer of adequate mortar), as well as the rehabilitation of the foundation of the north abutment (Figure 11) and the hydraulic protection of the south abutment using micro piles. Finally, repointing will be applied to the masonry on both faces of the bridge.

8. Conclusions

This paper presents a documentation-based methodology of numerical calculations with the purpose of understanding the structural behaviour of a historical stone arched bridge, interpreting its pathology, and—on this ground—proposing interventions for its preservation. The main conclusions of this work are as follows:

1. The exhaustive documentation of the bridge offers a sound basis for the understanding of its behaviour and, by way of consequence, for the formulation of protective measures for its preservation. The validity of this conclusion can be extended to all historical constructions and monuments;
2. The structural history of the bridge, based on historical sources, as well as "imprinted" on the construction itself, has dictated a methodology of numerical calculations following the construction phases of the monument step-by-step, as well as the effects of the major event of its man-induced damage one century ago. It was documented that if this step-by-step procedure had not been followed, the action–effects (stresses and deformations) would have been unrealistic, and it would have been impossible to interpret the damage to and the behaviour of the bridge. This step-by-step procedure was also dictated by the pronounced geometrical asymmetry of the bridge, as well as by the significantly different conditions of the foundation soil in the two abutments. It is, therefore, adequate for other arch bridges too that present similar asymmetries;
3. A series of parametric analyses of the geometrically accurate numerical model, although elastic and, hence, simplified, have allowed for the effect of the timber grids within the solid abutments to be interpreted, for the observed damage to be numerically confirmed and for the structural role of the RC jacket at the intrados of the bridge to be understood;
4. Based on the entire work, the large margin of safety of the bridge under its self-weight, as well as against flood was proven. The simplified investigation of the seismic behaviour of the bridge, dictated by the constraints related to the allowable interventions, has shown that the bridge meets the current Code requirements for a design earthquake, although some local damage is to be expected;
5. The approved scheme of interventions includes measures that alter neither the structural system of the bridge nor its appearance. More specifically, the RC jacket at the intrados is reconstructed using durable materials, the surveyed cracks are grouted and the foundation of the bridge is protected against scouring;
6. A final conclusion is related to the treatment of interventions using concrete (plain or reinforced) quite frequently applied to historical stone bridges in the past. Although nowadays, in conformity with international Charters, such interventions would not be acceptable, it is to be admitted that the repair of the bridge of Konitsa by the engineers of the French Army has contributed to the survival of the bridge. Nonetheless, as the durability of the early concretes is questionable, the modern engineer is asked to either protect the in situ concrete or replace it with durable materials compatible with the original ones.

Author Contributions: Conceptualisation, C.G., V.P. and E.V.; methodology, C.G. and E.V.; software, C.G. and E.O.; validation, C.G., E.V. and V.P.; writing—original draft preparation, C.G.; writing—review and editing, all; supervision, E.V.; project administration, V.P.; funding acquisition, E.V. All authors have read and agreed to the published version of the manuscript.

Funding: This research was funded by the Prefecture of Epirus, in the framework of a Contract among the Prefecture of Epirus, the Municipality of Konitsa, the Hellenic Ministry of Culture and the National Technical University of Athens.

Data Availability Statement: The data presented in this study are available on request from the corresponding author.

Acknowledgments: The assistance of A. Papaspyrou (Mayor of Konitsa), and V. Kaskanis (Director of the Service of Modern Monuments and Technical Works of Epirus, North Ionian and West Macedonia, Hellenic Ministry of Culture) are gratefully acknowledged.

Conflicts of Interest: The authors declare no conflicts of interest.

References

1. Casarin, F.; Bellin, S.; Mocellini, M.; Fabris, R. Static and seismic assessment of Ponte delle Capre, a masonry arch bridge. In *Life-Cycle of Structures and Infrastructure Systems*; Biondini, F., Frangopol, D.M., Eds.; Taylor & Francis: London, UK, 2023; pp. 1323–1330. [CrossRef]
2. Di Prisco, M.; Scola, M.; Zani, G. On site assessment of Azzone Visconti bridge in Lecco: Limits and reliability of current techniques. *Constr. Build. Mater.* **2019**, *209*, 269–282. [CrossRef]
3. Lubowiecka, I.; Arias, P.; Riveiro, B.; Solla, M. Multidisciplinary approach to the assessment of historic structures based on the case of a masonry bridge in Galicia (Spain). *Comput. Struct.* **2011**, *89*, 1615–1627. [CrossRef]
4. Martinelli, P.; Galli, A.; Barazzetti, L.; Colombo, M.; Felicetti, R.; Previtali, M.; Roncoroni, F.; Scola, M.; Prisco, M. Bearing capacity assessment of a 14th century arch bridge in Lecco (Italy). *Int. J. Archit. Herit.* **2018**, *12*, 237–256. [CrossRef]
5. Aydin, A.C.; Ozkaya, S.G. The finite element analysis of collapse of single-spanned historic masonry arch bridges (Ordu Sarpdere Bridge). *Eng. Fail. Anal.* **2018**, *84*, 131–138. [CrossRef]
6. Costa, C.; Arêde, A.; Morais, M.; Aníb, A. Detailed FE and DE modelling of stone masonry arch bridges for the assessment of load-carrying capacity. *Procedia Eng.* **2015**, *114*, 854–861. [CrossRef]
7. Franck, S.A.; Bretscneider, N.; Slowik, V. Safety analysis of existing arch bridges by nonlinear finite element simulations. *Int. J. Damage Mech.* **2020**, *29*, 126–143. [CrossRef]
8. Frunzio, G.; Monaco, M.; Gesualdo, A. 3D F.E.M. analysis of a Roman arch bridge. In Proceedings of the Historical Constructions, Guimaraes, Portugal, 7–9 November 2001; pp. 591–598.
9. Karalar, M.; Yesil, M. Implications of Arch Warp Altitudes on an Ancient Masonry Bridge under Ground Movements. *Appl. Sci.* **2023**, *13*, 7395. [CrossRef]
10. Zani, G.; Martinelli, P.; Galli, A.; Prisco, M. Three-dimensional modelling of a multi-span masonry arch bridge: Influence of soil compressibility on the structural response under vertical static loads. *Eng. Struct.* **2020**, *221*, 110998. [CrossRef]
11. Bayraktar, A.; Altunisik, A.C.; Birinci, F.; Sevim, B.; Turker, T. Finite-Element Analysis and Vibration Testing of a Two-Span Masonry Arch Bridge. *J. Perform. Constr. Facil.* **2010**, *24*, 46–52. [CrossRef]
12. Costa, C.; Ribeiro, D.; Silva, P.; Arede, A.; Calcada, R. Calibration of the numerical model of a stone masonry railway bridge based on experimentally identified modal parameters. *Eng. Struct.* **2016**, *123*, 354–371. [CrossRef]
13. Borlenghi, P.; Saisi, A.; Gentile, C. Effects of changing temperature in the vibration-based model updating of a masonry bridge. In *Life-Cycle of Structures and Infrastructure Systems*; Biondini, F., Frangopol, D.M., Eds.; Taylor & Francis: London, UK, 2023; pp. 1552–1559. [CrossRef]
14. Toth, A.R.; Orban, Z.; Bagi, K. Discrete element analysis of a stone masonry arch. *Mech. Res. Commun.* **2009**, *36*, 469–480. [CrossRef]
15. Lourenço, P.B.; Hunegn, T.; Medeiros, P.; Peixinho, N. Testing and analysis of masonry arches subjected to impact loads. In Proceedings of the ARCH'10—6th International Conference on Arch Bridges, Fuzhou, China, 11–13 October 2010; pp. 603–610.
16. Drosopoulos, G.A.; Stavroulakis, G.E.; Massalas, C.V. Limit analysis of a single span masonry bridge with unilateral frictional contact interfaces. *Eng. Struct.* **2006**, *28*, 1864–1873. [CrossRef]
17. Kiyono, J.; Furukama, A. Seismic Assesment of Stone Arched Bridges. In Proceedings of the 15th World Conference on Earthquake Engineering, Lisboa, Portugal, 24–28 September 2012.
18. Proske, D.; Gelder, P. *Safety of Historical Stone Arch Bridges*, 1st ed.; Springer: Berlin/Heidelberg, Germany, 2009; pp. 99–163, ISBN 978-3-540-77616-1. [CrossRef]
19. Scheibmeir, E. Nonlinear Seismic Analysis of a Masonry Arch Bridge. Master's Thesis, Universitat Politècnica de Catalunya, Barcelona, Spain, 2012.
20. Bencardino, F.; Curto, R.; Scavelli, V. Inspection and Structural Rehabilitation of an Existing Masonry Arch Railway Bridge. *Appl. Sci.* **2023**, *13*, 2973. [CrossRef]
21. Li-Ling, Y.; Zhi-Qian, D.; Gang, L. Simplified mechanical models for the seismic collapse performance prediction of unreinforced masonry structures. *Eng. Struct.* **2022**, *258*, 114131. [CrossRef]
22. Pelà, L.; Aprile, A.; Benedetti, A. Seismic assessment of masonry arch bridges. *Eng. Struct.* **2009**, *31*, 1777–1788. [CrossRef]
23. Pelà, L.; Aprile, A.; Benedetti, A. Comparison of seismic assessment procedures for masonry arch bridges. *Constr. Build. Mater.* **2013**, *38*, 381–394. [CrossRef]
24. Saygili, O.; Lemos, J.V. Influence of site effects on the seismic vulnerability of masonry arch bridges. In *Life-Cycle of Structures and Infrastructure Systems*; CRC Press: Boca Raton, FL, USA, 2023; pp. 1523–1529. [CrossRef]
25. Palieraki, V.; Oikonomopoulou, E.; Nikolopoulou, V.; Vintzileou, E.; Giannelos, C. The Historical Bridge of Konitsa-Epirus, Greece: Documentation of the Structural System. *Int. J. Archit. Herit.* **2022**, *17*, 1446–1463. [CrossRef]

26. Michaelidis, G. *Technical Report of Geodetic, Topographic and Photogrammetric Survey on the Arched Bridge of Konitsa*; Service of Modern Monuments and Technical Works of Epirus: North Ionian and West Macedonia, Greece, 2017. (In Greek)
27. Goutos, C. Old Bridges in our province. *Konitsa Mag.* **2014**, *179*, 419. (In Greek)
28. Giannelos, C.; Plainis, P.; Vintzileou, E. The historical bridge of Plaka: Interpretation of structural behavior and collapse. *Eng. Fail. Anal.* **2023**, *153*, 107589. [CrossRef]
29. Giannelos, C.; Vintzileou, E. The Rehabilitation of the Historical Bridge of Konitsa: A Documentation-Based Investigation of Structural Behaviour. In Proceedings of the PROHITECH 2021, Athens, Greece, 25–27 October 2021; Vayas, I., Mazzolani, F.M., Eds.; Lecture Notes in Civil Engineering. Springer: Berlin/Heidelberg, Germany, 2009.
30. SOFiSTiK. *Finite Element Method Software, version 14.14-30*; Sofistik AG: Nürnberg, Germany, 2014.
31. *EN 1996-1-1: 2005*; Eurocode 6: Design of Masonry Structures—Part 1-1: General Rules for Reinforced and Unreinforced Masonry structures. European Committee for Standardization: Brussels, Belgium, 2005.
32. Tassios, T.P.; Chronopoulos, M. Aseismic Dimensioning of Interventions on Low Strength Masonry Buildings. In Proceedings of the Middle East and Mediterranean Regional Conference on Low-Strength Masonry in Seismic Areas, Ankara, Turkey, 31 August—6 September 1986; Middle East University: Ankara, Turkey, 1986.
33. Tassios, T.P.; Mamillan, M. *Valutazione Strutturale dei Monumenti Antichi*, 1st ed.; Edizione Kappa: Roma, Italy, 1985.
34. Vintzileou, E. Three-Leaf Masonry in Compression, before and after Grouting: A Review of Literature. *Int. J. Archit. Herit. Conserv. Anal. Restor.* **2011**, *5*, 513–553. [CrossRef]
35. *EN 1995-1-1: 2004*; Eurocode 5: Design of Timber Structures—Part 1-1: General—Common Rules and Rules for Buildings. European Commission for Standardization: Brussels, Belgium, 2004.
36. NTUA Research Team. *Restoration of the Konitsa Stone Bridge*. Research Report 2018. (In Greek)
37. Epirus—Konitza the Bridge © Boissonnas Archive. *Hellenic Ministry of Culture*; Copyright: MOMus-Museum of Photography of Thessaloniki: Thessaloniki, Greece. Available online: https://www.nhmuseum.gr/en/departments/into-the-museum-s-collection/item/8648-bridgeinepirusphotographiccopyfromaglassplateoffredboissonnasc1903-1923theglassplateisatthemuseumofphotographyinthessaloniki (accessed on 15 January 2024).
38. ISCARSAH Guidelines for the analysis, conservation and structural restoration of architectural heritage. Unpublished work, 2024.
39. Hellenic Ministry of Culture. Regulatory framework for the preparation of studies and the execution of works on immovable monuments. *Off. Gov. Gaz.* **2019**, 2837/B/5-7-2019. (In Greek)
40. Rhomaides, A.; Zeitz, F. *Balkan Wars 1912–1913 (Photographic Album)*, 2nd ed.; Kedros Publishing: Athens, Greece, 2008; ISBN 978-960-04-1683-1.
41. NTUA Interdisciplinary Research Team. *The Bridge of Plaka: The NTUA Work for Its Restoration*; National Technical University of Athens: Athens, Greece, 2018; ISBN 978-618-82612-4-2. (In Greek)
42. Institute of Engineering Seismology and Earthquake Engineering, Catalog of Seismicity of the Greek Area, Research Project Helpos. 20 September 2021. Available online: https://www.itsak.gr/db/data (accessed on 15 January 2024).
43. EPPO (Earthquake Planning and Protection Organization). *Hellenic Seismic Code (EAK 2000)*; Ministry of Environment Planning and Public Works: Athens, Greece, 2003.